

Impacts of Material Performance Indices and Length Scale Parameter on Thermoelastic Damping in Micro/Nanoplates Applying Modified Couple Stress Theory

R. RESMI*, V. SURESH BABU**, M. R. BAIJU***

*University of Kerala, LBS Institute of Technology for Women, Thiruvananthapuram, Kerala-695012, India, E-mails: resmilbs@gmail.com; resmi@lbsitw.ac.in

**APJ Abdul Kalam Technological University, College of Engineering Trivandrum, Kerala, India

***University of Kerala; Kerala Public Service Commission, India; Kerala-695004, India

crossref <http://dx.doi.org/10.5755/j02.mech.25841>

1. Introduction

In recent times, small structural components like micro/nanoplates are extensively used in microelectromechanical systems (*MEMS*) and nanoelectromechanical systems (*NEMS*) attributable to its distinct and finest characteristics [1]. Micro/nano type rectangular plate based resonators are universally used for far-ranging applications such as in fields like energy harvesting [2, 3], robotics[4, 5], mass sensing [6, 7], electronic filtering [8, 9], communication systems [10, 11], autonomous distribution systems [12, 13], aerospace industry [14, 15], navigation systems [16, 17] etc.

MEMS/NEMS based plate resonators combine both mechanical and electrical functionalities on micro/nanoscales. Attributable to the surplus advantages like miniaturization, fractional weight, high surface to volume ratio, truncated energy consumption, adequate accuracy and precision, augmented sensitivity, enhanced reliability and acceptable stability of micro/nano plate type resonators [18 - 20]; its uses range from civil to military ones [21-23].

As a consequence of its key features and advantages micro/nanoplate resonators have a wide range of applications as micro- and nanoscale sensors [22-26], actuators [27, 28], switches [29], pumps [30, 31], filters [32, 33] and microfluidic components [34].

Quality factor (*QF*) decides the sensitivity and resolution of micro-/nano systems when used in sensor industry [35, 36]. As far as communication systems in micron ranges are concerned, enhanced quality factors increase signal to noise ratio and reduce phase noise [37, 38]. A high quality factor in resonators is achieved by reducing the dominant energy dissipation mechanisms which can be classified as extrinsic and intrinsic ones. The extrinsic losses like anchor damping [39, 40] and squeeze film damping [41, 42] can be diminished by proper geometric design. Air damping is another extrinsic dissipation mechanism which can be eliminated by ensuring ultra vacuum operation [43, 44]. Unlike extrinsic dissipation mechanisms, intrinsic ones like thermoelastic damping (*TED*) are very laborious to control and seems to be dominant in limiting the maximum attainable quality factor of the resonators [45, 46]. Modeling of high-quality factor resonators/sensors at the micro- and nano scale, is an emerging need and the factors affecting thermoelastic dissipation mechanism that cause quality factor to decline must be identified. In vibrating structures like resonators, thermoelastic damping is a crucial dissipation mechanism which arises due to the thermal gradients generated

during the flexing of the elastic media. The thermal currents emanating from the compression and expansion of the elastic media causes irreversible energy dissipation which leads to energy losses and quality factor curtailment. Accordingly, thermoelastic damping is a very critical loss mechanism at micro and nano-scales which limits the maximum achievable quality factor in the resonator denoted by thermoelastic damping limited quality factor (*Q_{TED}*).

Consequently, research in thermoelastic damping which limits the maximum achievable quality factor in the resonator is an interesting area. The maximum attainable thermoelastic damping limited quality factor (*Q_{TEDmax}*) in different structures is investigated in various research works as in tuning fork resonators [47], laterally vibrating resonators [48], gyroscopic devices [49], micro/nano flexural thinbeams [50], thickbeams [51], laminated composite micro-mechanical beam resonators [52], functionally graded microbeams [53], carbon nano tubes [54], rectangular and circular microplate resonators [55-57] multi-layered microplates [58-60], functionally graded plates [60], rotating microdisks [62], microrings [63] etc.

In resonating structures, the most important performance parameter is its quality factor which gives a direct measurement of expended energy due to various losses. The assessment of mechanical energy dissipation as a consequence of thermoelastic damping and the related quality factor analysis are prime concerns for the researchers in the last few decades. The presence of thermoelastic damping as a major mechanical energy dissipation in microbeams is spotted firstly by Zener (1937). Zener quantified the energy losses due to thermoelastic damping in homogeneous, isotropic, Euler–Bernoulli beams associated with its internal friction and provided an analytical solution for the thermoelastic energy dissipation [64-66]. Landau and Lifshitz (1959) derived an exact expression for the attenuation coefficient attributed to thermoelastic damping but not able to provide the solution for governing equations [67]. The study of thermoelastic vibrations in single-crystal silicon and silicon nitride based micro-resonators at room temperature is carried out by Roszhart (1990) [68] and Yasumura et al. (1999) [69] respectively. Lifshitz (2000) contributed an exact expression for the energy dissipation corresponding to thermoelastic damping based on coupled thermoelasticity [70]. Experimental studies on thermoelastic damping of *MEMS* based resonating sensors like Gyros are organised by Amy Duwel (2003) [71].

The analysis of thermoelastic damping in microplates is an interesting issue in micro/nano systems. Nayfeh and Younis (2004) presented a model for micropates of general shapes and boundary conditions and governed an analytical expression for the quality factor due to thermoelastic damping [72]. Vogl G. W et al.(2005) developed a micromodel for clamped circular plates and found to be computationally strong for sufficiently modelling the electrically actuated plates [73]. Rao S.S. elaborated the theory, computational aspects and applications of vibrations in continuous systems [74]. Zhili Hao et al.(2008) conducted an analytical study on thermoelastic damping in the contour-mode vibrations of micro/nanoscale circular plate resonators using a thermal-energy approach [75]. Zhang et al. (2008) presented theoretical analysis of thin plates formed by functionally graded materials formulated on physical neutral surface [76]. Yuxin Sun (2009) identified thermoelastic damping as a significant loss mechanism at room temperature in micro-scale circular plate resonators for axisymmetric vibrations [77]. Yi et al. (2010) analysed thermoelastic damping in contour-mode vibrations of micro- and nanoscale ring, disk, and elliptical plate resonators using finite element formulation [78]. Sun et al. (2010) derived the analytical expression for thermoelastic damping from the coupled thermoelastic problems of circular plates associated with the out of plane vibrations [79].

Ale Ali et al. (2011) studied thermoelastic damping in clamped-clamped annular micropates [80]. Li P. et al. (2012) developed an analytical model for investigating thermoelastic damping in the fully clamped and simply supported rectangular micropates [81]. Fang et al. (2013) investigated thermoelastic damping applying two-dimensional heat conduction in circular micropate resonators with axisymmetric vibration [82]. Zhikang Li et al. (2013) explored the resonant frequency of an electrostatically actuated micropate under uniform hydrostatic pressure [83]. A theoretical analysis of thermoelastic damping model in laminated tri layered circular plate resonators subjected to axisymmetric out-of-plane vibrations is conducted by Sun et al.(2014) [84]. Bogdan T. et al. (2014) analysed *TED* in auxetic plates[85]. J. N. Reddy et al. (2015). introduced the nonlinear finite element analysis [86]. Jiang et al. analysed the mechanism and model of thermoelastic damping in micropate resonators with three-dimensional heat conduction [87].

Zuo et al. (2016) governed analytical modeling of thermoelastic damping in bilayered micropate resonators[88]. Fang et al. (2017) explored thermoelastic damping in rectangular micropate resonators with three-dimensional heat conduction [89]. Ramu et al. (2017) analysed the free vibration characteristics of rotating *FGM* plates in high thermal environments using the finite element method [90]. The impacts of various parameters such as radius, rotating speed and power law index values on natural frequencies of rotating functionally graded material based plates are assessed. Liu et al. (2018) conducted theoretical analysis of thermoelastic damping in bilayered circular plate resonators with two-dimensional heat conduction [91]. The impacts of transverse and in-plane excitations on a simply supported piezoelectric rectangular thin plate and its dynamic responses are studied by Zhang et al (2018) [92]. From the study, the existence of chaotic wave motions and the chaotic dynamic responses on the four edged thin plates are proved. Liu et al. (2018) resolved the 3D model of thermoelastic

damping in laminated rectangular plate resonators for higher order modes [93]. Balakrishna Adhikari et al. (2019) examined the dynamic response of functionally graded plates employing a two-parameter-based elastic foundation model [94]. A quasi-3D theory is adopted to incorporate the non linear variation in the plates and the influence of diverse parameters on its dynamic response. Sayyid H. Hashemi et al. (2020) studied the free vibrations behaviour of viscoelastic functionally graded annular plates [95]. The perturbation technique is used to solve the equations of motion analytically and the natural frequencies of the plate are determined for different conditions. Kumar et al. (2020) studied thermoelastic damping in micro and nano-mechanical resonators applying entropy generation approach instead of complex frequency approach [96].

Abhik Sur et al. (2021) studied the influence of a moving heat source and magnetic field on a thick plate. The thermoelastic interactions subjected to varying magnetic field and temperature at different times are analysed [97]. Morteza Karimi et al. (2021) studied the wave propagation and vibration in double-layered magneto-electro-viscoelastic nanoplates to analyse the significance of surface layer changes according to modified couple stress [100]. Mehran Safarpour et al. (2021) investigated the frequency characteristics of a functionally graded graphene platelet reinforced composite porous circular/annular plates subjected to various boundary conditions [99]. Pawan Kumar et al. (2021) carried out the vibration response analysis of functionally graded piezoelectric porous plate with electro-thermal loading using finite element formulations [100]. The impact of magnitude and the applied voltage sign on the resulting frequency subjected to electric loading is also correlated. A parametric analysis has been done to enhance the natural frequencies of the plates.

When thermoelastic damping in micro/nanoresonators are considered, small scale effect caused by the rapid changes in properties on structural domain is very significant for predicting the related energy dissipation accurately. The size dependence effects of materials have been observed experimentally by scaling down the microstructure size [101, 102]. Accordingly, the size effect is essential in mechanical analyses of various structures for accurate prediction of thermoelastic damping. The classical theories are incapable of including the size effect at micron scales, hence, several higher order continuum theories are applied to relate stress and strain in resonating structures to evaluate the size dependencies. The primary non-classical continuum theory is couple stress theory (*CST*) which includes higher order theories developed by Mindlin [103], Toupin [104] and others including Koiter [105].

The accepted higher order theories employed to analyze the size scaling in microstructures are mainly micropolar theory [106], surface elastic theory [107], couple stress theory [108], strain gradient theory [109], nonlocal theory [110] and hybrid model like nonlocal strain gradient theory [111].

Micropolar elasticity theory includes both translation and rotation of local points whereas only translation motion is taken in classical elasticity theories. Micropolar elasticity suggest both couple stress and force stress for predicting the characteristics, but its main limitation lies in the fact that the rigid rotations did not have metrical importance and accordingly difficulty in the use of material symmetry precepts are experienced. The effect of surface stress on

micro/nanoresonators are modelled by surface elasticity theory and its main drawback is the requirement of a robust computational framework to solve the deformations and surface tension of microstructures.

According to the nonlocal elasticity theory introduced by Eringen, the state of stress at a given point in a material is dependent not only on the state of strain at that point but also on other points. The main limitation of nonlocal theory is that the concept is formed on an axisymmetric condition at local zones which is erroneous and reduces its accuracy. In couple stress models, higher order stresses are considered as the couple stresses. In classical couple stress theory, stretch and dilation gradients are not considered in making the constitutive analytical relations. Yang et al. introduced modified couple stress theory (*MCST*) with higher order equilibrium equations comprising conventional equilibrium equations of forces as well as moments of forces. While applying *MCST*, the size dependency is expressed by incorporating a single material length scale parameter. In modified strain gradient model, proposed by Lam et al., a set of higher-order metrics are used to describe the strain gradient model along with three length scale parameters to include rotation, dilation, and stretch gradients. From literature it is revealed that both *MSGT* and *MCST* provide almost the same results and so *MCST* is more advantageous due to its computational efficiency owing to a single material length scale parameter. Hence among the various higher order theories, the most commonly used is the Modified Couple Stress Theory (*MCST*) developed by Yang et al. The research works related to the study of vibrating structures with size effects are elaborated in succession.

Yang et al. (2002) developed couple stress based higher order theory for elasticity related to the deformation behaviour and size dependency [112]. According to this work, the two independent higher order material length scale parameters are reduced to simply one and formed a modified couple stress theory. Lam et al. (2003) developed higher order metrics to characterize strain gradient behaviors and number of independent elastic length scale parameters are reduced from five to three. Accordingly, a new strain gradient theory is evolved for analyzing the bending in plain beams [113]. Lim et al. (2004) studied the size dependent geometrically nonlinear response of thin elastic films with nano-scale thickness based on a continuum approach. The film was assumed elastically isotropic, and Kirchhoff's hypothesis was adopted to approximate the deformation kinetics [114]. Zhang et al. (2005) analysed inhomogeneities in strain gradient elasticity with couple stresses and corresponding issues for the effective property of composites [115].

A modification and generalization of the thin plate model developed in is evolved by P. Lu et al. (2006) which can be used for static and dynamic analysis of thin film structures [116]. They derived the governing equations of Kirchhoff and Mindlin plate models with surface effects. D. İeşan (2007) analysed thermoelasticity of bodies with microstructure and temperatures [117]. R. C. Batra et al. (2008) developed a reduced order model for an elliptic microplate with electrostatically actuation and clamped boundary condition based on the von Kármán nonlinearity and the Casimir force [118]. The bending analysis of strain gradient elastic micro-plates is conducted by K. A. Lazopoulos et al. (2009) [119]. L. Yin et al. (2010) conducted

vibration analysis of microscale plates based on modified couple stress theory [120].

The vibration analysis and size dependency of both rectangular and circular plates based on modified couple stress theory are conducted by E. Jomehzadeh et al. (2011) and the natural frequencies are presented [121]. Ke, Liao-liang et al. (2012) developed a non-classical microplate model for the axisymmetric nonlinear free vibration of Mindlin microplates made of functionally graded materials (*FGMs*) based on the modified couple stress theory [122]. Huu-Tai Thai et al. (2013) developed size-dependent models for functionally graded Kirchhoff and Mindlin plates for analyzing the bending, buckling, and vibrations in the framework of modified couple stress theory [123]. Gheshlaghi et al. (2013) studied the size dependent damping in axisymmetric vibrations of circular nanoplates [124]. Asghari Met al. (2013) conducted size-dependent mechanical analyses for functionally graded microplates [125]. Shaat et al. (2014) developed a new Kirchhoff plate model to study the bending behavior of nano-sized plates, including surface energy and microstructure effects employing modified couple stress theory [126]. Guo et al. (2014) analysed thermoelastic dissipation in circular micro-plate resonators using the generalized thermoelasticity theory [127]. Tsias et al. (2014) analysed the size effect on the static, dynamic and buckling analysis of orthotropic Kirchhoff-type skew micro-plates based on modified couple stress theory [128]. Ansari R. et al. (2014) studied the size-dependent vibrational behavior of functionally graded (FG) rectangular Mindlin microplates including geometrical non-linearity [129]. Farokhi et al. (2014) analysed nonlinear dynamic behaviour of a geometrically imperfect microplate based on the modified couple stress theory [130]. An eigen value analysis is also organized to get the natural frequencies with various geometric imperfections. Askari et al. (2015) organized vibrational analysis of clamped Kirchhoff microplates and conducted a parametric study to investigate the natural frequency of plates [131]. Şimşek, M. et al. (2015) studied the size-dependent vibration of a microplate under the action of a moving load based on the modified couple stress theory [132]. Eshraghi, Iman et al. (2015) conducted the static and free vibration analysis of functionally graded annular and circular micro-plates applying *MCST* [133]. Taati et al. (2015) analysed the size dependent buckling and post buckling behaviour of functionally graded micro-plates under different kinds of traction employing modified couple stress theory [134]. Lou Jia et al. (2015) presented a unified higher order shear deformable plate theory for functionally graded microplates by adopting *MCST* [135].

J. N. Reddy et al. (2016) conducted a nonlinear finite element analysis of functionally graded circular plates with modified couple stress theory [136]. Razavilar et al. (2016) analysed thermoelastic damping in rectangular microplate resonator using modified couple stress theory [137]. The authors explored the relation between quality factor and temperature for gold microplates. Ansari, R. et al. (2016) introduced a non-classical plate model to study the forced vibration of functionally graded microplates exposed to a harmonic excitation transverse force applying modified couple stress theory [138]. Askari et al. (2016) also conducted a parametric study and analysed the size-dependent dynamic pull-in in geometric non-linear micro-plates based on the same theory [139]. Nguyen et al. (2016) conducted isogeometric analysis associated with a novel quasi-3D

shear deformation theory to explore the size scaling in functionally graded microplates [140].

Thai et al. (2017) developed a numerical model for studying the shear deformation effects with size-dependent analyses of functionally graded microplates using modified strain gradient theory [141]. Liu et al. (2017) analysed the size effects of functionally graded moderately thick microplates using isogeometric analysis [142]. Malikan et al. (2017) analyzed the electro-mechanical shear buckling of piezoelectric nanoplate using modified couple stress theory based on simplified first order shear deformation theory [143].

Borjalilou et al. (2018) explored the small-scale effects on the thermoelastic damping in microplates applying strain gradient theory and the impacts of certain parameters on thermoelastic damping is analysed [144]. Thai (2018) et al. presented a non-classical model for bending, free vibration and buckling analyses of functionally graded (*FG*) isotropic and sandwich microplates based on the modified couple stress theory *MCST* and the refined higher order shear deformation theory [145]. Ajri, M et al. (2018) conducted nonlinear free vibration of viscoelastic nanoplate based on *MCST*. The impact of relaxation coefficient of the material on frequency, vibration amplitude and damping ratio of nanoplate is explored [146]. Kim et al. (2018) obtained the bending, free vibration, and buckling response of functionally graded porous micro-plates using the classical and first-order shear deformation plate theories [147]. Devi S. et al. (2018) analysed the vibrations of thermoelastic plate resonators based on Kirchhoff- Love plate theory. Damping and frequency shift in microscale plates are investigated based on *MCST* [148].

Farzam Amir et al. (2019) investigated the bending, buckling and free vibration behaviors of in-plane functionally graded porous microplates by means of isogeometric analysis (*IGA*) and modified couple stress theory [149]. The effect of porosity and other parameters are examined numerically by using hyperbolic shear deformation theory. Liu Y et al. (2019) analysed the size-dependent free vibration and buckling of three-dimensional graphene based microshells applying *MCST* [150]. Resmi R. et al. (2019) analysed the thermoelastic damping dependent quality factor analysis of rectangular plates applying modified coupled stress theory and the figure of merit of resonators are found out by numerical simulations. The significant parameters such as attenuation and frequency shifts are derived [151].

Thermoelastic damping analysis for size-dependent microplate resonators utilizing the modified couple stress theory and the three phase-lag heat conduction model Borjalilou et al. (2020) studied the thermoelastic damping in microplates according to strain gradient theory and a number of parametric studies has been conducted to assess the impact of *TED* [152]. Kumar R. et al. (2020) portrayed the significance of memory-dependent derivative approach for the analysis of thermoelastic damping in micromechanical resonators [153]. Devi S. et al. (2020) explored the thermoelastic damping and frequency shift of Kirchhoff plate resonators based on *MCST* and a computer algorithm is generated to obtain the numerical results [154]. Yekani, S. M. A. et al. (2020) presented a Levy type solution for bending, buckling, and vibration analyses of rectangular isotropic Mindlin micro plates based on the modified couple stress and first-order shear deformation plate theories [155]. Zhao-hai Yang et al. (2021) assessed thermoelastic damping in

rectangular nanoplates by including the size effects using nonlocal elasticity theory by using complex frequency approach [156]. Zhou et al. (2021) analysed thermoelastic damping in rectangular and circular micro/nanoplate resonators using nonlocal theory [157]. Resmi R. et al. (2021) investigated the significance of dimensionless length scale parameter on material dependent thermoelastic attenuation and frequency shifts of rectangular microplate resonators [158]. Xiao Ge et al. (2021) analysed the damping due to thermoelasticity in rectangular micro/nanoplates based on modified nonlocal strain gradient theory [159]. Yuan et al. (2021) conducted the post buckling analysis of nano shells based on surface elasticity theory [160]. Caiyuan Xiao et al. (2021) also explored the size dependent *TED* in circular nanoplates in structural domain by using nonlocal elasticity theory. The time-harmonic and asymmetric form for deflection and temperature change are chosen for extracting the natural frequency of circular plate resonators [161].

From the literature review, *TED* study and analysis in micro/nano rectangular plates using five different structural materials (polySi, diamond, Si, GaAs, and SiC) under various conditions for reduction of energy dissipation and optimization of quality factor is not available. The major purpose of the analysis is to attempt to fill this gap by exploring *TED* on isotropic rectangular micro-plates based on the Kirchhoff model. Non classical elasticity theory like *MCST* is used to enquire size dependency on thermoelastic damping because of its simplicity and accuracy as discussed in the previous section. Towards enhancing the thermoelastic damping limited quality factor, several optimizations are made on the basis of geometry and materials. *MEMS* and *NEMS* plates can be made of various materials, such as metals, polymers, semiconductors, and even functionally graded (*FG*) materials. Q_{TED} is predominantly optimized by properly selecting the structural material and dimensions, of the resonator. Selection of proper vibrating modes and boundary conditions also enhances Q_{TED} albeit to a lesser extent.

The governing equations of motion are derived by conforming to the Hamilton principle and the coupled heat conduction equation is employed to formulate the thermoelastic damping limited quality factors of the plates. Using complex frequency approach, from the real and imaginary parts of the frequency, an expression for quality factor is derived incorporating size effects. Hence a closed-form expression comprising small-scale characteristic parameters is derived to quantify *TED*. A comparison is made between the results extracted based on present nonclassical model (*MCST*) and those provided via classical (*LR*) formulation. The significance of capturing size effect and the influences of the different parameters, such as material length scale parameter, material properties, boundary conditions and the mode switching are investigated in the current analysis. The critical length (L_c), which corresponds to the peak energy dissipation under the abovementioned conditions is also explored. The impacts of material properties, size scaling, boundary conditions and mode switching using both *LR* theory and *MCST* is analysed.

In the current analysis, the analytical expressions for thermoelastic dissipation of Kirchhoff's rectangular micro/nanoplates based on both classical (*LR*) and nonclassical (*MCST*) continuum theories are presented. The analytical expressions including material performance indices and size effects corresponding to thermoelastic damping limited

quality factor are evolved based on complex frequency approach as follows. The influence of material length scale parameters, structural material properties, boundary types and mode switching on thermoelastic damping limited quality factor and critical length is investigated in subsequent sections. The numerical results obtained for both classical and nonclassical theories are compared for both Q_{TED} and L_c . The variation of thermoelastic energy dissipation with length of the micro/nanoplate follows a Lorentzian behaviour for all specified conditions and applicable to both classical and nonclassical theories even if the magnitude is different.

In this paper, Section 2 gives the basic formulation of *MCST* according to Yang. In Section 3, the expressions for the thermoelastic damping limited quality factor of *MCST* are derived in terms of the Lifschitz and Roukes expressions for the thermoelastic damping limited quality factor of classical thermoelasticity. Section 4 presents the results and discussions, in which the various techniques for enhancing Q_{TED} are analyzed quantitatively by applying *MCST*. The impacts of size scaling, mode switching, boundary conditions, material properties, and the internal length scale parameter are discussed in Section 4. The conclusions of the work are given in Section 5.

2. Formulation of basic equations

2.1. Basic formulation of MCST

Unlike non-classical continuum theories, in classical elasticity theory, stress and strain energy depends only on the strain tensor and rotation gradients are not considered.

In *MCST* Yang et al. and Rao et al., a higher order equilibrium condition is applied to predict the size dependencies at micro/nano scales. The total strain energy is considered as a quadratic function of the symmetric strain tensor (conjugated with stress tensor) and the symmetric curvature tensor (conjugated with couple stress tensor) where the latter one is the additional measure of deformation.

To interpret the size effect related to the material microstructures, a single material length scale is developed in *MCST* based on Kirchhoff plate model.

In a deformed isotropic linear elastic material occupying region \tilde{A} , the strain energy E is given by:

$$U = \int_{\tilde{A}} (\sigma_{ij} \varepsilon_{ij} + m_{ij} \eta_{ij}) d\tilde{A} \quad (i, j = 1, 2, 3). \quad (1)$$

Eq. (1) shows that the deformation energy density does not depend explicitly on the anti-symmetric part of displacement gradient and the anti-symmetric part of rotation gradient. Only the symmetric part of displacement gradient conventional star in tensor and the symmetric part of rotation gradient (symmetric curvature tensor) contribute to the deformation energy. The rotation vector and the anti-symmetric curvature tensor do not contribute to the deformation energy. The strain tensor and symmetric curvature tensor are the deformation measures conjugate to the symmetric stress tensor σ and the deviatoric couple stress tensor m , respectively. The different tensors are defined by couple stress which can be determined from torsion tests of slim cylinders or bending tests of thin beams in microscale.

Symmetric part of Cauchy's stress tensor:

$$\sigma_{ij} = \lambda tr(\varepsilon_{ij}) I + 2\mu \varepsilon_{ij}. \quad (2)$$

Strain tensor:

$$\varepsilon_{ij} = \frac{1}{2} [\nabla u + (\nabla u)^T]. \quad (3)$$

Deviatoric part of symmetric couple stress tensor:

$$m_{ij} = 2l^2 \mu \chi_{ij}. \quad (4)$$

Deviatoric part of symmetric curvature tensor:

$$\chi_{ij} = \frac{1}{2} [\nabla \psi + (\nabla \psi)^T], \quad (5)$$

where: μ is the displacement vector; Lamé's constants are $\lambda = Ev / np$; $\mu = \frac{E}{2n}$ where: E , ν are the Young's modulus and Poisson's ratio of the plate material respectively. According to *MCST*, to characterize size effect a material length scale parameter l is adapted and estimated from the structural material property. In addition to the conventional parameters, two new material dependent parameters p and n are introduced, which are derived from Poisson's ratio and as shown in Table 2.

Infinitesimal rotation vector:

$$\psi_i = \frac{1}{2} curl(u_i). \quad (6)$$

From Eqs. (3) and (5), the strain tensor ε_{ij} and curvature tensor χ_{ij} are symmetric, and consequently from Eqs. (2) and (4), the stress tensor σ_{ij} and couple stress tensor m_{ij} are also symmetric.

The schematic diagram of a microplate of length a , width b and thickness h defined in the rectangular coordinate system is shown in Fig. 1. When a thin plate is considered for analysis, it is assumed to be under plane stress condition and the thickness, h and width, b of the plate is taken to be small as compared to length a i.e., $b < 5h$.

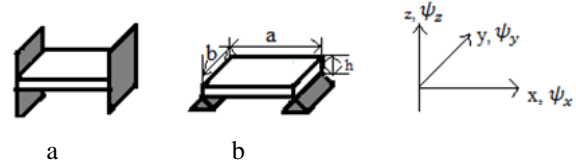


Fig. 1 Schematic diagram of a microplate with different boundary types: a) Clamped – clamped; b) Simply supported

2.2. Governing equations of motion and coupled thermoelasticity of microplates

Let ψ_x and ψ_y denote the transverse normal rotations about y and x axis,

$$\left. \begin{aligned} \psi_x(x, t) &= -\frac{\partial W(x, y, t)}{\partial x} \\ \psi_y(x, t) &= -\frac{\partial W(x, y, t)}{\partial y} \\ u_x &= -zW(x, y, t) \end{aligned} \right\}. \quad (7)$$

According to Kirchoff's plate theory, the displacement field (u_x, u_y, u_z) of an arbitrary point (x, y, z) is given by:

$$\left. \begin{aligned} u_x &= z\psi_x(x, t) = -z \frac{\partial W(x, y, t)}{\partial x} \\ u_y &= z\psi_y(x, t) = -z \frac{\partial W(x, y, t)}{\partial y} \\ u_z &= W(x, y, t) \end{aligned} \right\}, \quad (8)$$

where: $W(x, y, t)$ denotes transverse deflection of the microplate.

From Eqs. (1) and (2), rotation vector ψ can be rewritten as:

$$\left. \begin{aligned} \psi_x &= \frac{1}{2} \left(\frac{\partial u_z}{\partial y} - \frac{\partial u_y}{\partial z} \right) = \frac{1}{2} W_{,y} \\ \psi_y &= \frac{1}{2} \left(\frac{\partial u_x}{\partial z} - \frac{\partial u_z}{\partial x} \right) = -\frac{1}{2} W_{,x} \\ \psi_z &= \frac{1}{2} \left(\frac{\partial u_y}{\partial x} - \frac{\partial u_x}{\partial y} \right) = -\frac{z}{2} W_{,xy} \end{aligned} \right\}. \quad (9)$$

The symmetric rotation gradient tensor, χ_{ij} can be expanded by using Eq. (5) as $\chi_{ij} = \frac{1}{2} [\nabla \psi + (\nabla \psi)^T]$.

Non-zero components of symmetric part of the rotation gradient tensors are:

$$\left. \begin{aligned} \chi_{xx}^s &= W_{,xy} \\ \chi_{yy}^s &= -W_{,xy} \\ \chi_{xy}^s &= \frac{1}{2} (W_{,yy} - W_{,xx}) \\ \chi_{zz} &= \chi_{yz} = \chi_{zx} = 0 \end{aligned} \right\}. \quad (10)$$

The non-zero components of the strain are:

$$\left. \begin{aligned} \varepsilon_{xx} &= -z W_{,xx} \\ \varepsilon_{yy} &= -z W_{,yy} \\ \varepsilon_{xy} &= -z W_{,xy} \end{aligned} \right\}. \quad (11)$$

Stress-strain relationships for thermoelastic materials:

$$\begin{aligned} \varepsilon_{xx} &= \frac{1}{E} (\sigma_{xx} - \nu \sigma_{yy}) + \alpha_t (T - T_0) = \\ &= \frac{1}{E} \left(\sigma_{xx} + \frac{(m-n)}{2} \sigma_{yy} \right) + \alpha_t (T - T_0), \end{aligned} \quad (12)$$

$$\begin{aligned} \varepsilon_{yy} &= \frac{1}{E} (\sigma_{yy} - \nu \sigma_{xx}) + \alpha_t (T - T_0) = \\ &= \frac{1}{E} \left(\sigma_{yy} + \frac{(m-n)}{2} \sigma_{xx} \right) + \alpha_t (T - T_0), \end{aligned} \quad (13)$$

$$\begin{aligned} \varepsilon_{zz} &= \frac{\nu}{E} (\sigma_{xx} + \sigma_{yy}) + \alpha_t (T - T_0) = \\ &= \frac{(n-m)}{2E} (\sigma_{xx} + \sigma_{yy}) + \alpha_t (T - T_0). \end{aligned} \quad (14)$$

where: $m = \{0.774, 0.931, 0.72, 0.69, 0.808\}$ for polySi, diamond, Si, GaAs, SiC respectively which are derived from Poisson's ratio.

In rectangular plates, bending moments (m_{xx}, m_{yy}, m_{xy}) and torsion moments (Y_{xx}, Y_{yy}, Y_{xy}) exist and expressed as:

$$\left. \begin{aligned} m_{xx} &= \frac{El^2}{n} W_{,xy} \\ m_{yy} &= \frac{El^2}{n} W_{,xy} \\ m_{xy} &= \frac{El^2}{n} (W_{,yy} - W_{,xx}) \\ m_{zz} &= m_{yz} = m_{zx} = 0 \end{aligned} \right\}, \quad (15)$$

$$\left. \begin{aligned} Y_{xx} &= D \times [-zu_{z,xx} - \alpha\theta] \\ Y_{yy} &= D \times [-zu_{z,yy} - \alpha\theta] \\ Y_{xy} &= -\frac{E}{n} Zu_{z,xy} \end{aligned} \right\}, \quad (16)$$

$$\text{where: } D = \frac{Em}{np}.$$

Including size effects, the strain energy is:

$$E = \frac{1}{2} \int_0^a \int_0^b \int_{-h/2}^{h/2} \left(\frac{Dz}{h^2} F_1 + \frac{E}{n} F_2 \right) dx dy dz, \quad (17)$$

$$F_1 = W_{,xx}^2 + W_{,yy}^2 + \alpha\theta (W_{,xx} + W_{,yy})$$

$$\text{where: } F_2 = W_{,xy}^2 \left(\left(\frac{z}{h} \right)^2 + \left(\frac{l}{h} \right)^2 \right) + \left(\frac{l}{h} \right)^2 (W_{,yy} - W_{,xx})^2 \quad \text{and}$$

kinetic energy of the microplate is:

$$K = \frac{1}{2} \int_0^a \int_0^b \left\{ \rho h \dot{W}^2 + \frac{\rho h^3}{12} [\dot{\psi}_x^2 + \dot{\psi}_y^2] \right\} dx dy, \quad (18)$$

where: ρ is the density of the plate material.

According to the variational principle:

$$\delta \left\{ \int_{t_1}^{t_2} (K - U) dt \right\} = 0, \quad (19)$$

For clamped - clamped and simply supported rectangular microplates, the integral of the Gaussian curvature is zero [79], where:

$$\int_0^a \int_0^b [W_{,xx} W_{,yy} - W_{,xy}^2] dx dy = 0. \quad (20)$$

The moment of inertia:

$$I_T = \frac{12\alpha}{h^3} \int_{-h/2}^{h/2} z \theta dz. \quad (21)$$

The dynamic governing equation of the microplate in terms of $W(x, t)$ is given by:

$$(B + B') \nabla^4 W + \frac{B}{2} \nabla^2 I_T - \rho h \ddot{W} = 0, \quad (22)$$

where: $\nabla^2 = \frac{\partial^2}{\partial x^2} + \frac{\partial^2}{\partial y^2}$; $\nabla^4 = \frac{\partial^4}{\partial x^4} + \frac{2\partial^4}{\partial x\partial y} + \frac{\partial^4}{\partial y^4}$; $B = Dh^3$; $B' = Dl^2 h \frac{p}{2m}$.

The temperature distribution in the microplate due to the thermoelastic coupling is:

$$\dot{\theta} = \chi \nabla^2 \theta - \frac{\alpha E_b T}{p C_V} \frac{\partial}{\partial t} \sum_i \varepsilon_{ij}, \quad (23)$$

where: C_V is the heat capacity coefficient at constant volume; χ is the thermal diffusivity of the solid.

The linearized version of the heat equation is:

$$\left(1 + 2\dot{r} \frac{n}{p}\right) \dot{\theta} = \chi \theta_{,zz} + z \frac{\dot{r}}{\alpha} (\dot{W}_{,xx} + \dot{W}_{,yy}), \quad (24)$$

where the relaxation strength of the thermoelastic solid is $\dot{r} = (E_{ad} - E) / E = E\alpha^2 T_0 / \rho C p$, where E_{ad} is the unrelaxed or adiabatic value of Young's modulus; E is its relaxed or isothermal value.

3. Solution of the thermoelastic equation and MCST based quality factor

The solutions of equation of motion and coupled heat equation are:

$$\left. \begin{aligned} W(x, y, t) &= w_0(x, y) e^{i\omega t} \\ \theta(x, y, z, t) &= \theta_0(x, y, z) e^{i\omega t} \end{aligned} \right\}. \quad (25)$$

The temperature profile in microplate is derived as:

$$\theta_0(x, y, z) = \frac{\dot{r}}{\alpha} (w_{0,xx} + w_{0,yy}) \left[z - \frac{\sin(gz)}{g \cos(gh/2)} \right]. \quad (26)$$

The thermal moment of inertia can be given by:

$$I_T = \frac{12\dot{r}}{h^3} \left[\frac{h^3}{12} + \frac{h}{g^2} - \frac{2}{g^3} \tan\left(\frac{hg}{2}\right) \right] \nabla^2 \omega_0. \quad (27)$$

Using Eqs. (26) and (27) in (22), the equation of motion will be:

$$\left(B + B' + \frac{B}{2} \dot{r} (1 + f(\omega)) \right) \nabla^4 W - \rho h \ddot{W} = 0, \quad (28)$$

where:

$$f(\omega) = f(g(\omega)) = \frac{24}{h^3 g^3} \left[\frac{hg}{2} - \tan\left(\frac{hg}{2}\right) \right]. \quad (29)$$

Isothermal value of eigen frequency of the microplate:

$$\omega_0 = \begin{cases} \pi^2 \sqrt{\frac{B}{\rho h}} \left(\frac{m_1^2}{a^2} + \frac{m_2^2}{b^2} \right); \text{ for } SS \\ \pi^2 \sqrt{\frac{B}{\rho h}} \left(\frac{\left(m_1 + \frac{1}{2}\right)^2}{a^2} + \frac{\left(m_2 + \frac{1}{2}\right)^2}{b^2} \right); \text{ for } CC \end{cases} \quad \text{and}$$

$$\left(\frac{\omega}{\omega_0} \right)^2 = 1 + \frac{B'}{B} + \frac{\dot{r}}{2} [1 + f(\omega)]. \quad (30)$$

From the above equation, the frequency is complex and expressed as:

$$\begin{aligned} \text{Re}(\omega) &= \omega_0 \times \\ &\times \left[\frac{\sqrt{B}}{4} + \frac{\dot{r}}{\sqrt{B}} \left(1 - \frac{6}{\xi^3} \frac{\sinh \sinh(\xi) + \sin \sin(\xi)}{\cosh \cosh(\xi) + \cos \cos(\xi)} \right) \right], \end{aligned} \quad (31)$$

$$\begin{aligned} \text{Im}(\omega) &= \omega_0 \frac{4\dot{r}}{B} \times \\ &\times \left(\frac{6}{\xi^3} \frac{\sinh \sinh(\xi) + \sin \sin(\xi)}{\cosh \cosh(\xi) + \cos \cos(\xi)} - \frac{6}{\xi^2} \right). \end{aligned} \quad (32)$$

where:

$$\xi = b \sqrt{\frac{\omega_0}{2\chi}}, \quad (33)$$

and

$$B = 16 \left(1 + \frac{B'}{B} \right). \quad (34)$$

TED in terms of inverse of quality factor is expressed as:

$$Q^{-1} = 2 \frac{|Im(\omega)|}{|Re(\omega)|}. \quad (35)$$

In the analysis:

$$\begin{aligned} Q_{MCST}^{-1} &= \\ &= \frac{2\dot{r} \left(\frac{6}{\xi^3} \frac{\sinh \sinh(\xi) + \sin \sin(\xi)}{\cosh \cosh(\xi) + \cos \cos(\xi)} - \frac{6}{\xi^2} \right)}{B^2 \left(\frac{B}{16} + \frac{\dot{r}}{\sqrt{B}} \left[1 - \frac{6}{\xi^3} \frac{\sinh \sinh(\xi) + \sin \sin(\xi)}{\cosh \cosh(\xi) + \cos \cos(\xi)} \right] \right)}, \end{aligned} \quad (36)$$

According to Lifshitz and Roukes assumption, Eq. (36) is reduced to the well-known Lifshitz and Roukes expression as follows when size effect was not included:

$$Q_{LR}^{-1} = \dot{\gamma} \left(\frac{6}{\xi^3} \frac{\sinh\sinh(\xi) + \sin\sin(\xi)}{\cosh\cosh(\xi) + \cos\cos(\xi)} - \frac{6}{\xi^2} \right). \quad (37)$$

Q_{MCST}^{-1} in terms of Q_{LR}^{-1} is expressed as:

$$Q_{MCST}^{-1} = \frac{2Q_{LR}^{-1}}{\dot{\gamma} \left(\frac{6}{\xi^3} \frac{\sinh\sinh(\xi) - \sin\sin(\xi)}{\cosh\cosh(\xi) + \cos\cos(\xi)} - 1 \right) - \frac{B}{4}}. \quad (38)$$

4. Results and discussions

In this section, the numerical results are presented by simulating the analytical expressions corresponding to the thermoelastic energy dissipation allied with classical theory (Lifshitz and Rouke's theory) and modified couple stress theory (MCST) as given in the derived equations. The analytical expressions are numerically simulated by using MATLAB 2015. The impacts of structural material properties, material length scale parameters, boundary conditions and mode switching on thermoelastic damping limited quality factor and critical length of Kirchhoff's micro/nanoplates based on both higher order theory, modified couple stress theory (MCST) and classical theory (LR) are assessed.

To validate the analytical study, microplate resonators of length $a = 200 \mu\text{m}$; width $b = 200 \mu\text{m}$; thickness $h = 10 \mu\text{m}$ using five different structural materials (polySi, diamond, GaAs, SiC and Si) are examined at temperature $T = 298 \text{ K}$. The experimentally reported mechanical and thermodynamic properties of all the structural materials are given in Table 1. The mechanical boundary conditions selected for analysis include simply supported and clamped-clamped boundary types. The Kirchhoff's plates are analysed for first two modes designated as (1,1) and (1,2) to investigate the influence of mode switching.

Table 1

Mechanical and thermal properties of structural materials at $T_0=298 \text{ K}$

Materials	Parameters					
	$E, \text{ GPa}$	ν	ρ	k	C_p	$\alpha, 10^{-6}$
PolySi	150	0.226	2328	40	713	2.3
Diamond	800	0.069	3515	100	510	1.2
Si	130	0.28	2230	90	699	2.59
GaAs	85.9	0.31	5316	52	550	5.73
SiC	415	0.192	3200	70	937.5	3.0

4.1. Quality factor analysis

Analysis of the thermoelastic damping limited quality factor (Q_{TED}) of micro- and nanoplates is discussed in this section for various material length scale parameters, structural materials, boundary conditions and mode switching applying both classical (LR) and nonclassical (MCST) theories.

Table 2 describes the numerical values of Q_{TED} obtained by the simulations using MATLAB 2015 under three diverse material length scale parameters ($l = 0, 0.5, 1$). The numerical results are computed for the five different

structural materials (Si, polySi, GaAs, SiC and diamond) and two boundary types (simply supported and clamped-clamped). All the specified conditions are analysed for two different modes- (1,1) and (2,1) also. The numerical results are differentiated for both classical (LR) and non-classical theories (MCST) to evaluate the thermoelastic damping limited quality factor accurately, presuming the specified conditions as delineated in the subsequent sections.

Table 2

Values of thermoelastic damping limited quality factor (Q_{TED}) of a microplate obtained numerically for various structural materials {Boundary conditions-simply supported and clamped-clamped; length scale parameters ($l(\mu\text{m}) = 0, 0.5$ and 1) and vibrating modes M-I(1,1) and M-II(2,1)}

$l, \mu\text{m}$	Material	PolySi	Diamond	Si	GaAs	SiC
0	SS	7055.17	5248.79	6028.81	3496.87	2709.44
	CC	7055.17	5248.79	6028.82	3496.87	2709.44
0.5	SS	8418.22	6563.40	7037.79	4025.44	3271.60
	CC	8418.21	6563.40	7037.79	4025.44	3271.61
1	SS	12140.19	10084.81	9820.28	5492.69	4799.38
	CC	12140.19	10084.81	9820.28	5492.69	4799.38
0	SS	7056.03	5249.11	6029.10	3497.03	2709.98
	CC	7056.02	5249.10	6028.99	3497.02	2709.97
0.5	SS	8418.99	6563.89	7037.91	4026.12	3272.21
	CC	8418.98	6563.89	7037.89	4025.99	3272.20
1	SS	12140.79	10085.11	9820.97	5492.99	4799.92
	CC	12140.77	10085.09	9820.86	5492.81	4799.89

4.1.1. Effects of material length scale parameter

Intending to assess the influence of material length scale parameter on Q_{TED} , the micro/nanoplates are subjected to various material length scale values like 0, 0.5 and 1. The classical theory is realized by designating $l = 0$ in the investigation. The values of material length scale parameters chosen for integrating MCST are 0.5 and 1.

Fig. 2 shows the variation of thermoelastic energy dissipation with the length of a simply supported plate applying different material length scale parameters i.e. $l = 0, 0.5$ and 1 . The dissipation curves are plotted for micro/nanoplates of all the five selected structural materials with simply supported mechanical boundary type and vibrating in first mode (1,1).

As a result of selecting higher values of material length scale parameters, thermoelastic dissipation diminishes as depicted in Fig. 2.

Table 2 shows the Q_{TED} values of micro- and nanoplates with different length scale parameters for the five structural materials. As shown in Table 2, as the length-scale parameter increases, the thermoelastic damping limited quality factor of all materials increases in the order $Q_{TED} (l = 0 \mu\text{m}) < Q_{TED} (l = 0.5 \mu\text{m}) < Q_{TED} (l = 1 \mu\text{m})$; the same is validated as shown Fig. 3. The variation of thermoelastic damping limited quality factor with l , for both simply supported and clamped-clamped boundary types are also presented. The divergence in Q_{TED} with length scale parameter for both boundary type is the same i.e. as l increases, Q_{TED} increases. For all vibrating modes of the resonator, as l increases Q_{TED} also increases.

To ascertain the impact of material length scale parameter on Q_{TED} more accurately, a quantitative analysis is done by computing the percentage difference of Q_{TED}

attained between the various values of l . Table 3 presents the percentage change in Q_{TED} between different length scale parameters. The transitions in l considered for investigation are 0-0.5, 0.5-1 and 0-1.

From Table 3, the maximum percentage difference is obtained for the switching of $l = 0$ to $l = 1$ for micro/nanoplates using all the structural materials. The maximum percentage difference (92.13 %) in Q_{TED} is obtained for diamond based plates when MCST is applied instead of classical theory (i.e., $l = 0 \mu\text{m}$ to $l = 1 \mu\text{m}$).

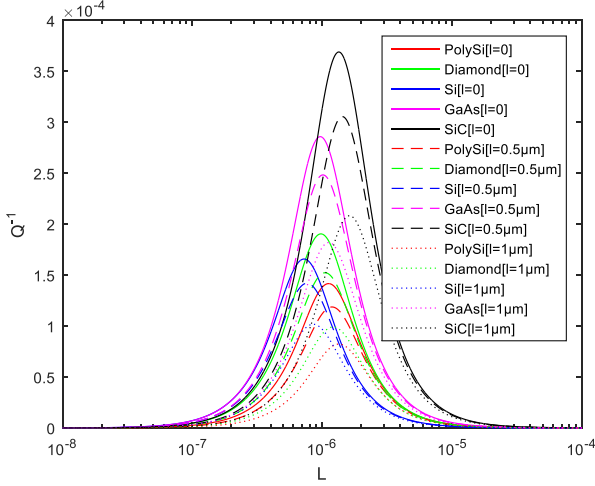


Fig. 2 Thermoelastic energy dissipation Q^{-1} versus length L of a simply supported microplate for different length scale parameters applying various structural materials

Table 3

Percentage difference between different length scale parameters of various structural materials

$l, \mu\text{m}$	PolySi	Diamond	Si	GaAs	SiC
0-0.5	19.32	25.04	16.73	15.11	20.74
0.5-1	44.21	53.65	39.54	36.44	46.69
0-1	72.07	92.13	62.88	57.07	77.13

4.1.2. Effects of material performance indices

In view of the investigation of thermoelastic energy dissipation based on structural material properties, the dissipation curves of micro/nano plates are plotted against length as shown in Fig. 3. It is remarkable that the structural material properties dominate the thermoelastic energy loss very much and the dependency is mainly due to a material performance index called thermoelastic damping index, TDI .

The amount of thermoelastic damping is material-dependent, because energy dissipation is determined by the material's mechanical and thermal properties. Energy dissipation of the resonator depends on the relaxation strength \hat{r} of the resonator; $\hat{r} = \frac{E\alpha^2 T_0}{\rho C_p}$, which depends on an important material performance index parameter known as the thermoelastic damping index $TDI = \frac{E\alpha^2}{C_p}$. The main factor

affecting the total energy dissipation and QF of the resonator is TDI . The relaxation strength can be expressed in terms of TDI : i.e. $\hat{r} = TDI * \frac{T_0}{r}$. SiC suffers large energy losses

because of high TDI and relaxation strength values leading to high thermoelastic damping and low Q_{TED} values. Among the various structural materials selected for analysis, TDI value is the lowest for polySi and the maximum value for Q_{TED} is attained as shown in Table 3.

From Fig. 3, the maximum Q_{TED} (12140.19) is obtained for a clamped-clamped micro- or nanoplate with polySi as the structural material. From Fig. 3, the order of materials in which Q_{TED} decreases is obtained as Q_{TED} polySi > Q_{TED} diamond > Q_{TED} Si > Q_{TED} GaAs > Q_{TED} SiC, as shown in Table 3. The variation of thermoelastic damping limited quality factor is inversely related to the material performance index parameter, thermoelastic damping index generally, as shown in Table 4.

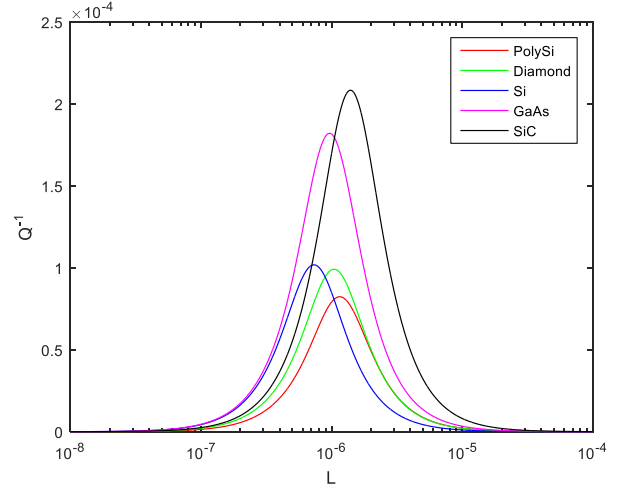


Fig. 3 Thermoelastic energy dissipation Q^{-1} versus length L of a clamped-clamped microplate for different structural materials vibrating in (1,1) mode

Table 4

Material dependent performance indices for rectangular plates

Materials	Material Performance Index Parameters						
	$TDI, 10^{-6}$	l_T, nm	$\chi, \text{cm}^2/\text{s}$	p^*	q^{**}	k^{***}	C_V
PolySi	1113	3	0.241	0.774	1.226	0.548	1659864
Diamond	2651	3.69	0.558	0.931	1.069	0.862	1792650
Si	1248	7.56	0.577	0.72	1.28	0.44	1558770
GaAs	5128	4.42	0.178	0.69	1.31	0.38	2923800
SiC	3984	2.04	0.233	0.808	1.192	0.616	3000000

* $(1-\nu)$, ** $(1+\nu)$, *** $(1-2\nu)$

The descending order in which Q_{TED} diminishes among the different structural materials is polySi > Si > GaAs > SiC, which is inversely related to TDI usually, as shown in Table 3. i.e. the sequential order in which Q_{TED} drops off is Q_{TED} polySi > Q_{TED} Si > Q_{TED} diamond > Q_{TED} GaAs > Q_{TED} SiC for both boundary conditions for lower values of material length scale parameter.

4.1.3. Effects of boundary conditions

The thermoelastic damping limited quality factor is quantified for two boundary types (simply supported and clamped-clamped) of the micro/nanoplates. Fig. 4 demonstrates the thermoelastic energy dissipation curves of the micro/nanoplates using five structural materials for both

boundary types. The resonating mode selected for the plate is (1,1) i.e. first mode and the length scale parameter, $l=1$.

For the simply supported and clamped-clamped support conditions of the plates, it is identified that the change in Q_{TED} with different boundary conditions is negligible. While analyzing the tabulated table for thermoelastic damping limited quality factor, the maximum Q_{TED} (12140.19) is obtained for a simply supported polySi based plate. From Table 2 it is also verified that the material order of diminishing Q_{TED} is independent of the boundary types i.e. the sequential order in which Q_{TED} drops off is Q_{TED} polySi $>$ Q_{TED} Si $>$ Q_{TED} diamond $>$ Q_{TED} GaAs $>$ Q_{TED} SiC for both boundary conditions.

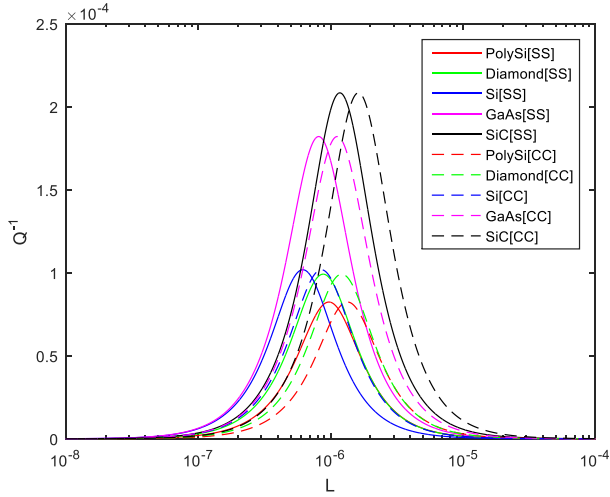


Fig. 4 Thermoelastic energy dissipation Q^{-1} versus length L of a microplate for various boundary conditions (simply supported and clamped-clamped) and structural materials

4.1.4. Effect of mode switching

Fig. 5 demonstrates the variation of thermoelastic energy dissipation with length of micro/nanoplates vibrating in different modes.

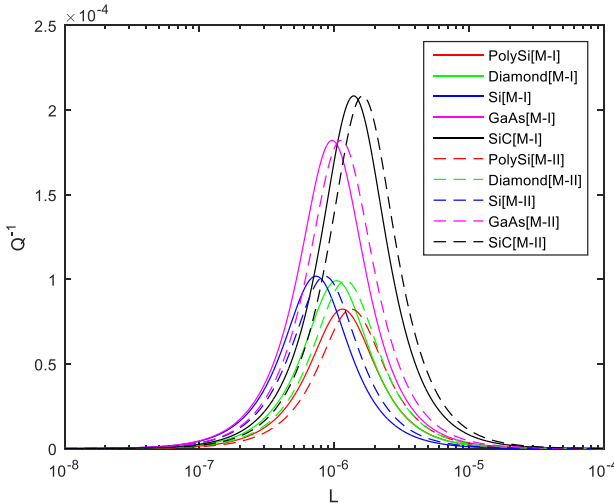


Fig. 5 Thermoelastic energy dissipation Q^{-1} versus length L of a microplate for various vibrating modes (M-I(1,1) and M-II(2,1)) and structural materials

The two modes selected for analysis are MI-(1,1) and M-II (2,1) and the impact is investigated for all the structural materials chosen as shown in Fig. 5. The mechanical boundary type opted for investigation is the clamped-

clamped type with length scale parameter $l=1\mu\text{m}$. On account of mode switching, the divergence of Q_{TED} is negligible as in the case of change in boundary types.

4.2. Critical length analysis

Critical length L_c , is an important design parameter in micro/nanoplate resonators that represents the length at which peaking of energy occur and consequently included in the current investigation. The prior awareness of the critical length of the micro/nanoplate helps the designer of micro/nano plate resonators to diminish energy losses by properly selecting the dimensions. The analysis is conducted by comprehending the classical (LR) and nonclassical ($MCST$) theories and comparing the numerical results attained for L_c under the st. In the analysis, LR theory is included by setting $l=0$ and the $MCST$ is incorporated by selecting nonzero values of length scale parameter i.e. $l=0.5$ and 1 . The outcomes of integrating material length scale parameters, different boundary types and mode switching are investigated in the micro/nanoplates using five various structural materials. Table 5 shows the critical length values of micro/nanoplates for both LR and $MCST$ theories under the specified conditions.

Table 5

Values of thermoelastic critical length L_c of a microplate obtained for various structural materials under two vibrating modes M-I(1,1) and M-II(2,1) with varying length scale parameters (l (μm) = 0, 0.5 and 1) and boundary conditions (simply supported and clamped-clamped)

MODE	$l, \mu\text{m}$	B.C	PolySi	Diamond	Si	GaAs	SiC
(1,1)	0	SS	0.64	0.55	0.41	0.55	0.76
		CC	0.96	0.83	0.62	0.83	1.15
	0.5	SS	0.68	0.60	0.43	0.58	0.81
		CC	1.02	0.90	0.65	0.87	1.22
	1	SS	0.76	0.69	0.48	0.64	0.93
		CC	1.15	1.04	0.73	0.96	1.39
(2,1)	0	SS	0.81	0.70	0.52	0.70	0.97
		CC	1.12	0.97	0.72	0.96	1.34
	0.5	SS	0.86	0.76	0.55	0.73	1.03
		CC	1.18	1.05	0.76	1.01	1.42
	1	SS	0.97	0.88	0.61	0.81	1.17
		CC	1.34	1.21	0.85	1.12	1.62

4.2.1. Effect of material length scale parameter

The influence of material length scale parameter is investigated by designating various values for material length scale parameter, l . The different values of length scale parameter chosen for investigation are 0, 0.5 and 1. Fig. 6 depicts the normalized thermoelastic energy dissipation curve of a simply supported micro/nanoplate, plotted against its length, L . The resonating plates are vibrating in first mode with different material length scale values.

On examining Table 5, the significance of l is substantiated i.e. as the value of l increases, critical length also increases. The increasing order of critical length is L_c ($l=0.2\mu\text{m}$) $<$ L_c ($l=0.5\mu\text{m}$) $<$ L_c ($l=1\mu\text{m}$) as illustrated in Fig 6. The maximum value of critical length is obtained for SiC based resonator with $l=1$.

In the analysis, to quantify the impact of length scale parameter precisely, the percentage difference in L_c for selected transitions of length scale parameters are

summarised in Table 6. First-order natural frequencies of the microresonators obtained by ANSYS software.

The switching of l observed in the current analysis are 0-0.5, 0.5-1 and 0-1. The impact of material length scale parameter increases with the value of l . While the change over between various l are considered, the greatest impact is found for 0-1 transitions for clamped-clamped type rectangular plates.

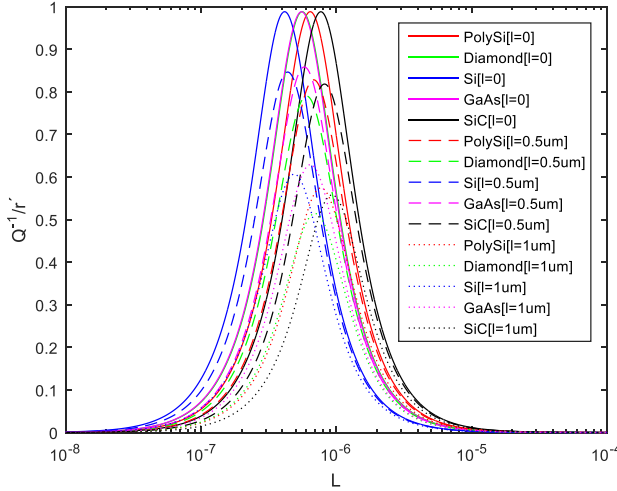


Fig. 6 Normalized thermoelastic energy dissipation Q^{-1} versus length L of a microplate applying various structural materials and length scale parameters ($l=0 \mu\text{m}$, $0.5 \mu\text{m}$ and $1 \mu\text{m}$)

Table 6

Percentage difference of critical length between different length scale parameters

MODE	$l, \mu\text{m}$	B.C	PolySi	Diamond	Si	GaAs	SiC
(1,1)	0-0.5	SS	6.06	8.70	4.76	5.31	6.37
		CC	6.06	8.09	4.72	4.71	5.9
	0.5-1	SS	11.11	13.95	10.99	9.84	13.79
		CC	11.98	14.43	11.59	9.84	13.03
	0-1	SS	19.78	24.32	17.59	16.27	21.09
		CC	19.85	24.31	17.65	16.26	20.98
(2,1)	0-0.5	SS	5.99	8.22	5.61	4.20	6.00
		CC	5.22	7.92	5.41	5.08	5.80
	0.5-1	SS	12.02	14.63	10.34	10.38	12.73
		CC	12.7	14.16	11.18	10.33	13.16
	0-1	SS	17.98	22.78	15.93	14.57	18.69
		CC	17.89	22.02	16.56	15.38	18.92

4.2.2. Effects of material performance indices

Concerning the dependency of critical length L_c on material type, normalized thermoelastic energy dissipation curves are plotted against the length of micro/nanoplates with preferred structural materials.

Fig.7 illustrates the comparison between the critical length L_c of a clamped-clamped micro- or nanoplate using various structural materials vibrating in first mode with $l=1 \mu\text{m}$.

From Fig. 7, the maximum critical length is obtained for SiC based micro/nanoplates and the order of materials in which critical length diminishes is $\text{SiC} > \text{polySi} > \text{diamond} > \text{GaAs} > \text{Si}$. The most important finding regarding the sequential order in which L_c declines is its dependency on an important material performance index parameter, thermal diffusion length- l_T . It is substantiated that the trend is inversely proportional to the thermal diffusion length l_T .

noted from Table 4. The critical length is inversely proportional to the thermal diffusion length l_T ; the material order in which L_c change occurs is $L_c \text{ SiC} > L_c \text{ polySi} > L_c \text{ diamond} > L_c \text{ GaAs} > L_c \text{ Si}$.

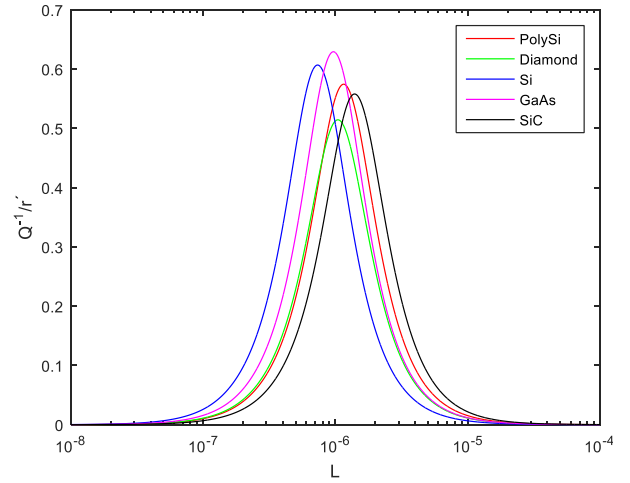


Fig. 7 Normalized thermoelastic energy dissipation Q^{-1} versus length L of a microplate for different structural materials vibrating in (1,1) mode

4.2.3. Effects of boundary conditions

The influence of two different boundary conditions-simply supported and clamped-clamped types on critical length are analyzed for the micro/nanoplates and plotted as shown in Fig. 8.

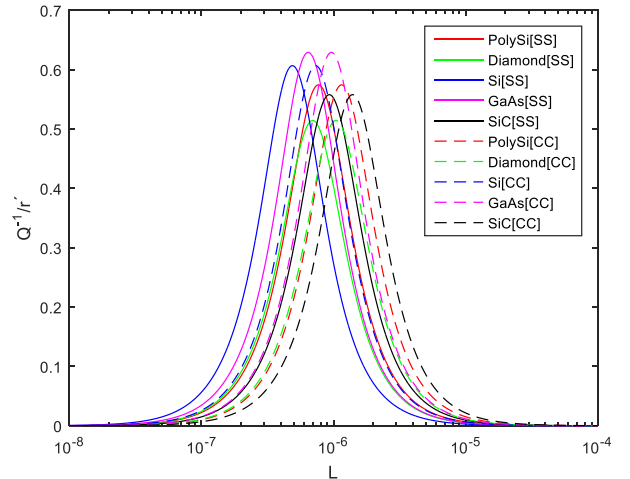


Fig. 8 Normalized thermoelastic energy dissipation Q^{-1} versus length L of a microplate with different boundary types (simply supported and clamped-clamped) applying various structural materials

The normalized thermoelastic energy dissipation curves of micro/nanoplates with simply supported and clamped-clamped boundary conditions applying all the selected structural materials are illustrated in Fig. 8.

As a result, a comparison of critical length of the micro/nanoplates with both boundary types using the five structural materials are realized. From Fig. 8., it is confirmed that a clamped-clamped plate shows more critical length than a simply supported plate as shown in Table 5.

All the energy dissipation curves are plotted for micro/nanoplates vibrating in first mode with length scale

parameter $l = 1 \mu\text{m}$. From Fig. 8, the maximum critical length ($1.62 \mu\text{m}$) seems to be obtained for SiC based clamped-clamped plates and can be verified from Table 5 also.

The significance of boundary conditions on various conditions is evaluated by analyzing the percentage difference in critical length by transforming simply supported boundary type to clamped clamped one with different structural materials, length scale parameters and modes as depicted in Table 7. From Table 7, it is proved that Si in (1,1) mode shows the maximum percentage difference of critical length (41.32 %) as the mechanical boundary type is converted from simply supported to clamped clamped type; vibrating in first mode with $l = 1 \mu\text{m}$

Table 7

Percentage difference of critical length between different boundary conditions

Mode	$l, \mu\text{m}$	PolySi	Diamond	Si	GaAs	SiC
(1,1)	0	40.00	40.58	40.78	40.58	40.84
	0.5	40.00	40.00	40.74	40	38.05
	1	40.84	40.46	41.32	40	39.66
(2,1)	0	32.12	20.47	32.26	31.33	32.03
	0.5	31.37	32.04	32.06	32.18	31.84
	1	32.03	31.58	32.88	32.12	32.26

4.2.4. Effects of mode switching

For the sake of mode changing analysis, two successive modes-M-I(1,1) and M-II (2,1) are selected for the vibrating micro/nanoplates as shown in Fig. 9.

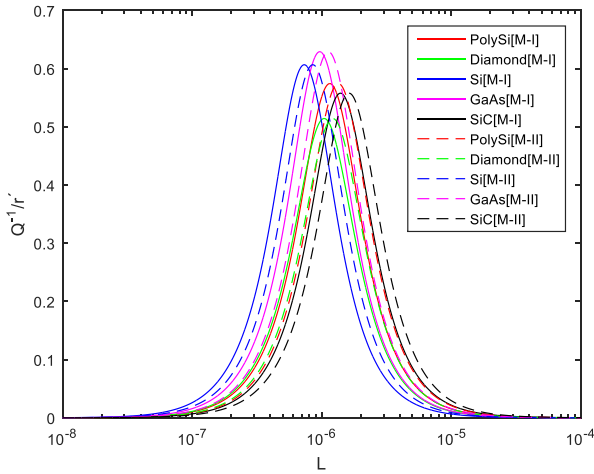


Fig. 9 Normalized thermoelastic energy dissipation Q^{-1} versus length L of a microplate vibrating in different modes (M-I(1,1) and M-II(2,1)) applying various structural materials

Table 8

Percentage difference of critical length between different modes

$l, \mu\text{m}$	B.C	PolySi	Diamond	Si	GaAs	SiC
0	SS	23.45	24	23.66	24	24.28
	CC	15.38	15.56	14.93	14.53	15.26
0.5	SS	23.38	23.53	24.49	22.90	23.91
	CC	14.55	15.38	15.60	14.89	15.15
1	SS	24.28	24.20	23.85	23.45	22.86
	CC	15.26	15.11	15.19	15.38	15.28

Fig. 9 depicts the normalized energy dissipation curves of a clamped-clamped microplate vibrating in two

different modes. The plots are represented for all the five structural materials with $l = 1 \mu\text{m}$. The comparison of critical length of micro/nanoplate for enhancing mode number is evident i.e.as the mode number increases, L_c also increases. The maximum critical length is obtained for SiC ($1.62 \mu\text{m}$) vibrating in M-II (2,1) mode as shown in Table 5.

To assess the impact of mode switching on L_c accurately, the percentage difference is calculated for the transformation of mode (1,1) to mode (2,1) and presented in Table 8.

The most important observation regarding the mode switching is that the micro/nanoplates with clamped-clamped boundary condition is less affected by the change in vibrating mode. The maximum and minimum percentage difference in L_c is obtained for plates with simply supported and clamped-clamped boundary conditions respectively.

5. Conclusions

In this work, the focus is to numerically analyze the impacts of structural material properties, boundary conditions, material length scale parameters and mode number increment on size dependent thermoelastic damping of vibrating isotropic Kirchhoff's micro/nanoplates. The numerical results are simulated from the attained analytical expressions of vibrating plates by using MATLAB R2015a. The analytical expressions for thermoelastic energy dissipation are derived in terms of material performance indices of the structural materials used and the specified conditions are investigated. The consequences on thermoelastic damping limited quality factor Q_{TED} and Critical Length L_c of micro/nanoplates are quantitatively evaluated and rationally presented. The essential outcomes are delineated as:

1. In view of all the structural materials selected (polySi, Si, GaAs, SiC and diamond), the maximum value of Q_{TED} is obtained for polySi based rectangular plates and verified to be essentially material dependent. As thermoelastic energy dissipation increases, Q_{TED} diminishes which is established to be related to a material performance parameter, thermoelastic damping index TDI . Maximum Q_{TED} is achieved with rectangular plates made up of polySi as the structural material having the minimum TDI factor. The energy dissipation is maximum for SiC based micro/nanoplates with maximum TDI among the five different structural materials. Considering critical length of the micro/nano rectangular plates, L_c is also validated to be relied on an important structural material thermal property known as thermal diffusion length. As the thermal diffusion length of the material increases, the length at which peaking of energy L_c occurs also increases. The maximum and minimum values of L_c are obtained for SiC and Si respectively. The thermal diffusion length of Si is the maximum and that of minimum is for SiC. Hence it is confirmed that Q_{TED} and L_c are dependent on two material performance indices - TDI factor and thermal diffusion length -in a reverse order.

2. The size dependency analysis of Kirchhoff's micro/nanoplates is included in the study by applying a higher order theory, modified couple stress theory, which consists of only one material length scale parameter l . The implication of classical theory is evaluated by selecting $l=0$ and the size dependency is estimated by designating different values of l as $0.2 \mu\text{m}$, $0.5 \mu\text{m}$ and $1 \mu\text{m}$. Analysis of the influence of

material length scale parameter l on the magnitude of thermoelastic energy dissipation discloses that the enhancement in Q_{TED} can be accomplished by opting higher values of l . In rectangular micro/nano plates, as the value of l increments, L_c also increases.

3. Considering the two theories-classical LR and non-classical $MCST$ ones, the impacts of mode number increment on thermoelastic energy dissipation and Q_{TED} are negligible for all the structural materials. Increasing the value of mode number i.e. when the micro/nano plates are vibrated at higher modes, L_c also increases which is an important observation regarding the plates.

4. Between the two boundary conditions, simply supported and clamped-clamped types of micro/nanoplates selected for analysis, the impact of mechanical boundary condition on TED and Q_{TED} is also negligible as in the case of mode switching. As far as L_c is analysed, the critical length is verified to be greater in clamped-clamped micro/nanoplates. The prior knowledge of Q_{TED} and L_c can help engineers to design high-performance, low-loss resonators at micro/nanoscales.

References

- Bongsang, K.; Candler, R.; Hopcroft, M.; Agarwal, M.; Park, W. T.; Li, J.; Kenny, T.** 2004. Investigation of MEMS resonator characteristics during long-term and wide temperature variation operation. <https://doi.org/10.1115/IMECE2004-61727>.
- Thakare, N.; Thakare, S.; Shahakar, R.** 2018. Ultrasonic frequency MEMS disk resonator for energy harvesting application, 3rd IEEE International Conference on Recent Trends in Electronics, Information & Communication Technology (RTEICT). <https://doi.org/10.1109/RTEICT42901.2018.9012602>
- Gratuze, M.; Alameh, A. H.; Nabki, F.** 2019. Design of the squared daisy: a multi-mode energy harvester, with reduced variability and a non-linear frequency Response, *Sensors* 19(15): 3247. <https://doi.org/10.3390/s19153247>.
- Duan, Q.; Du, Z.; Yu, H.; Wang, Y.; Dong, W.** 2016; Error analysis and experimental study of a bi-planar parallel mechanism in a pedicle screw robot system, *Sensors* 16(12):2022. <https://doi.org/10.3390/s16122022>.
- Zi, B.; Yin, G.; Zhang, D.** 2016. Design and optimization of a hybrid-driven waist rehabilitation robot, *Sensors* 16(12):2121. <https://doi.org/10.3390/s16122121>.
- Mouro, J.; Pinto, R.; Paoletti, P.; Tiribilli, B.** 2021. Microcantilever: dynamical response for mass sensing and fluid characterization, *Sensors* 21(1): 115. <https://doi.org/10.3390/s21010115>.
- Nazemi, H.; Antony Balasingam, J.; Swaminathan, S.; Ambrose, K.; Nathani, Mu.; Ahmadi, T.; Babu Lopez, Y.; Emadi, A.** 2020. Mass sensors based on capacitive and piezoelectric micromachined ultrasonic transducers – CMUT and PMUT, *Sensors* 20(7): 2010. <https://doi.org/10.3390/s20072010>.
- Park, H.; Chae, H.; Kim, J.** 2021. An optimal digital filtering technique for incremental delta-sigma ADCs using passive integrators, *Electronics* 10(2): 213. <https://doi.org/10.3390/electronics10020213>.
- Faseehuddin, M.; Herencsar, N.; Albrni, M. A.; Sampe, J.** 2021. Electronically tunable mixed-mode universal filter employing a single active block and a minimum number of passive components, *Applied Sciences* 11(1): 55. <https://doi.org/10.3390/app11010055>.
- Mehdi, M.; Ajani, M. T.; Tahir, H.; Tahir, S.; Alizai, Z.; Khan, F.; Riaz, Q.; Hussain, M.** 2021. PUF-based key generation scheme for secure group communication using MEMS, *Electronics* 10(14): 1691. <https://doi.org/10.3390/electronics10141691>.
- Bouchami, A.; Elsayed, M. Y.; Nabki, F.** 2019. A sub-mW 18-MHz MEMS oscillator based on a 98-dB Ω adjustable bandwidth transimpedance amplifier and a Lamé-Mode resonator, *Sensors* 19(12): 2680. <https://doi.org/10.3390/s19122680>.
- Valenzuela, A.; Simani, S.; Inga, E.** 2021. Automatic overcurrent protection coordination after distribution network reconfiguration based on peer-to-peer communication, *Energies* 14(11): 3253. <https://doi.org/10.3390/en14113253>.
- Tiete, J.; Domínguez, F.; Silva, B. D.; Segers, L.; Steenhaut, K.; Touhafi, A.** 2014. Sound compass: a distributed MEMS microphone array-based sensor for sound source localization, *Sensors* 14(2):1918-1949. <https://doi.org/10.3390/s140201918>.
- Hu, B.; Zhang, S.; Zhang, H.; Lv, W.; Zhang, C.; Lv, X.; San, H.** 2019. Fabrications of L-Band LiNbO₃-based SAW resonators for aerospace applications, *Micromachines* 10(6): 349. <https://doi.org/10.3390/mi10060349>Aerospaceapplications-
- Wang, H.; Liu, N.; Su, Z.; Li, Q.** 2019. Research on low-cost attitude estimation for MINS/Dual-antenna GNSS integrated navigation method, *Micromachines* 10(6): 362. <https://doi.org/10.3390/mi10060362>.
- Blocher, L.; et al.** 2021. Purely inertial navigation with a low-cost MEMS sensor array, *IEEE International Symposium on Inertial Sensors and Systems (INERTIAL)*, pp. 1-4. <https://doi.org/10.1109/INERTIAL51137.2021.9430468>.
- Du, S.; Gan, X.; Zhang, R.; Zhou, Z.** 2021. The integration of rotary MEMS INS and GNSS with artificial neural networks, *Mathematical Problems in Engineering* 2021: 6669682, 10 p. <https://doi.org/10.1155/2021/6669682>.
- Grüger, H.** 2021. MOEMS and MEMS - Technology, Benefits & Uses. <https://doi.org/10.1002/9781119636489.ch5>.
- Chen, Y. J.** 2013. Advantages of MEMS and its Distinct New Applications, *AMR* 813: 205–209. <https://doi.org/10.4028/www.scientific.net/amr.813.205>.
- Gammel, P.; Fischer, G.; Bouchaud, J.** 2005. RF MEMS and NEMS technology, devices, and applications, *Bell Labs Technical Journal* 10: 29-59. <https://doi.org/10.1002/bltj.20103>.
- Young, D.; Zorman, C.; Mehregany, M.** 2007. MEMS/NEMS Devices and Applications, *Bhushan B.*

- (eds) Springer Handbook of Nanotechnology. Springer Handbooks. Springer, Berlin, Heidelberg. https://doi.org/10.1007/978-3-540-29857-1_15.
22. **Lu, Y.; Yan, P.; Xiang, C.; Chen, D.; Wang, J.; Xie, B.; Chen, J.** 2019. A resonant pressure microsensors with the measurement range of 1 MPa based on sensitivities balanced dual resonators, *Sensors* 19(10): 2272. <https://doi.org/10.3390/s19102272>.
 23. **Liu, G.; Cao, W.; Zhang, G.; Wang, Z.; Tan, H.; Miao, J.; Li, Z.; Zhang, W.; Wang, R.** 2021. Design and simulation of flexible underwater acoustic sensor based on 3D buckling structure, *Micromachines* 12(12): 1536. <https://doi.org/10.3390/mi12121536>.
 24. **Mao, Q.; Jing, W.; Gao, W.; Wei, Z.; Tian, B.; Liu, M.; Ren, W.; Jiang, Z.** 2021. High-sensitivity enzymatic glucose sensor based on ZnO urchin-like nanostructure modified with Fe₃O₄ magnetic particles, *Micromachines* 12(8): 977. <https://doi.org/10.3390/mi12080977>.
 25. **Niranjan, A.; Gupta, P.; Rajoriya, M.** 2021. Piezoelectric MEMS micro-cantilever biosensor for detection of SARS-CoV2, *International Conference on Communication, Control and Information Sciences (ICCISc)*, pp. 1-5. <https://doi.org/10.1109/ICCISc52257.2021.9484976>.
 26. **Liu, Z.; Tian, B.; Zhang, B.; Zhang, Z.; Liu, J.; Zhao L.; Shi, P.; Lin, Q.; Jiang, Z.** 2021. High-performance temperature sensor by employing screen printing technology, *Micromachines* 12(8): 924. <https://doi.org/10.3390/mi12080924>.
 27. **Zhang, D.; Cai, A.; Zhao, Y.; Hu, T.** 2021. Macro modeling of V-shaped electro-thermal MEMS actuator with human error factor, *Micromachines* 12(6): 622. <https://doi.org/10.3390/mi12060622>.
 28. **Yin, Y.; Fang, Z.; Liu, Y.; Han, F.** 2019. Temperature-insensitive structure design of micromachined resonant accelerometers, *Sensors* 19(7): 1544. <https://doi.org/10.3390/s19071544>.
 29. **Peng, Y.; Sun, Y.; Luo, G.; Wu, G.; Zhang, T.** 2019. Recent advancements in inertial micro-switches, *Electronics* 8(6): 648. <https://doi.org/10.3390/electronics8060648>.
 30. **Bao, Q.; Zhang, J.; Tang, M.; Huang, Z.; Lai, L.; Huang, J.; Wu, C.** 2019. A novel PZT pump with built-in compliant structures, *Sensors* 19(6): 1301. <https://doi.org/10.3390/s19061301>.
 31. **Jenke, C.; Pallejà Rubio, J.; Kibler, S.; Häfner, J.; Richter, M.; Kutter, C.** 2017; The combination of micro diaphragm pumps and flow sensors for single stroke based liquid flow control, *Sensors* 17(4): 755. <https://doi.org/10.3390/s17040755>.
 32. **Linsa, M. L.; Resmi, R.** 2015. Analysis of variable substrate properties effects on electric field distribution in MEMS EVA tunable filters, *International Conference on Control, Instrumentation, Communication and Computational Technologies (ICCICCT)*, pp. 38-41. <https://doi.org/1109/ICCICCT.2015.7475245>.
 33. **Dousti, S. M.; Afrang, S.** 2021. MEMS tunable filters based on DGS and waveguide structures: a literature review, *Analog Integr Circ Sig Process* 108: 141–164. <https://doi.org/10.1007/s10470-021-01862-7>.
 34. **Liu Yoon, J. S.; Park, J.; Ahn H. R.; Yoo, S. J.; Kim Y. J.** 2021. Microfluidic airborne metal particle sensor using oil microcirculation for real-time and continuous monitoring of metal particle emission, *Micromachines* 12(7): 825. <https://doi.org/10.3390/mi12070825>.
 35. **Yin, Y. X.; Zhang, X. P.; Yin, X. J.; Li, Y.; Xu, X. R.; An, J. M.; Wu, Y. D.; Liu, X. P.; Zhang, D. M.** 2021. High-Q-factor tunable silica-based microring resonators, *Photonics* 8(7): 256. <https://doi.org/10.3390/photonics8070256>.
 36. **Banerjee, S.; Nath, U.; Dutta, P.; Jha, A. V.; Apasani, B.; Bizon, N.** 2021. A theoretical terahertz metamaterial absorber structure with a high quality factor using two circular ring resonators for biomedical sensing, *Inventions* 6(4): 78. <https://doi.org/10.3390/inventions6040078>.
 37. **Trzpil, W.; Maurin, N.; Rousseau, R.; Ayache, D.; Vicet, A.; Bahriz, M.** 2021. Analytic optimization of cantilevers for photoacoustic gas sensor with capacitive transduction, *Sensors* 21(4): 1489. <https://doi.org/10.3390/s21041489>.
 38. **Moradian, S.; Akhkandi, P.; Huang, J.; Gong, X.; Abdolvand, R.** 2021. A battery-less wireless respiratory sensor using micro-machined thin-film piezoelectric resonators, *Micromachines* 12(4): 363. <https://doi.org/10.3390/mi12040363>.
 39. **Resmi, R.; Baiju, M. R.; Babu, V. S.** 2017. Material dependent thermoelastic damping limited quality factor analysis of disc resonators, *International conference of Electronics, Communication and Aerospace Technology (ICECA)*, pp. 675-680, <https://doi.org/10.1109/ICECA.2017.8212750>.
 40. **Vukasin, G. D.; et al.** 2019. Effect of substrate thickness on anchor damping in MEMS devices, *20th International Conference on Solid-State Sensors, Actuators and Microsystems & Eurosensors XXXIII (Transducers & Eurosensors XXXIII)*, pp. 1843-1845. <https://doi.org/10.1109/TRANSDUCERS.2019.8808424>.
 41. **Finny, S.; Resmi, R.** 2016 Material and geometry optimization for squeeze film damping in a micromirror, *International Conference on Emerging Technological Trends (ICETT)*, pp. 1-5. <https://doi.org/10.1109/ICETT.2016.7873698>.
 42. **Kaur, Iqbal; Lata, Parveen; Singh, Kulvinder.** 2021. Study of frequency shift and thermoelastic damping in transversely isotropic nano-beam with GN III theory and two temperature, *Archive of Applied Mechanics* 91: 1-15. <https://doi.org/10.1007/s00419-020-01848-3>.
 43. **Zhang, C.; Xu, G.; Jiang, Q.** 2003. Analysis of the air-damping effect on a micromachined beam resonator, *Mathematics and Mechanics of Solids* 8(3): 315-325. <https://doi.org/10.1177/1081286503008003006>.
 44. **Zhang, X.; Tang, W. C.** 1994. Viscous air damping in laterally driven microresonators, *Proceedings IEEE Micro Electro Mechanical Systems an Investigation of Micro Structures, Sensors, Actuators, Machines and Robotic Systems*, pp. 199-204, <https://doi.org/10.1109/MEMSYS.1994.555623>.
 45. **Resmi, R.; Suresh Babu, V.; Baiju, M. R.** 2021. Numerical study of thermoelastic damping effects on

- diamond based beams with plane stress and plane strain conditions applying nonclassical elasticity theory, *Advances in Dynamical Systems and Applications* 16(2): 1371-1379.
46. **Serdean, F.; Pustan, M.; Dulescu, C.; Birleanu, C.; Serdean M.** 2020. Analysis of the thermoelastic damping effect in electrostatically actuated MEMS resonators, *Mathematics* 8(7):1124. <https://doi.org/10.3390/math8071124>.
 47. **Zega, V.; Frangi, A.; Guercilena, A.; Gattere, G.** 2018. Analysis of frequency stability and thermoelastic effects for slotted tuning fork MEMS resonators, *Sensors* 18(7): 2157. <https://doi.org/10.3390/s18072157>.
 48. **Tu, C.; Lee, J. Y.; Zhang, X. S.** 2020. Dissipation analysis methods and Q-enhancement strategies in piezoelectric MEMS laterally vibrating resonators: a review, *Sensors* 20(17): 4978. <https://doi.org/10.3390/s20174978>.
 49. **Li, C.; Gao, S.; Niu, S.; Liu, H.** 2016. Study of intrinsic dissipation due to thermoelastic coupling in gyroscope resonators, *Sensors* 16(9): 1445. <https://doi.org/10.3390/s16091445>.
 50. **Srikar, V. T.; Senturia, S. D.** 2002. Thermoelastic damping in fine grained polysilicon flexural beam resonators, *J. Microelectromech. Syst.* 11(5): 499–504.
 51. **Parayil, D. V.; Kulkarni, S. S.; Pawaskar, D. N.** 2015. Analytical and numerical solutions for thick beams with thermoelastic damping, *Int. J. Mech. Sci.* 94: 10–19.
 52. **Srikar Vengallatore.** 2005. Analysis of thermoelastic damping in laminated composite micromechanical beam resonators, *J. Micromech. Microeng.*, pp. 2398-2404.
 53. **Li, X.; Li, L.; Hu, Y.; Ding, Z.; Deng, W.** 2017. Bending, buckling and vibration of axially functionally graded beams based on nonlocal strain gradient theory, *Composite Structures* 165: 250–265.
 54. **Pradiptya, I.; Ouakad, H. M.** 2018. Size-dependent behavior of slacked carbon nanotube actuator based on the higher-order strain gradient theory, *Int. J. Mech. Mater. Des.* 14(3): 393–415. <https://doi.org/1007/s10999-017-9382-5>.
 55. **Resmi, R.; Suresh Babu, V.; Baiju, M. R.** 2021. Impact of dimensionless length scale parameter on material dependent thermoelastic attenuation and study of frequency shifts of rectangular microplate resonators, *IOP Conf. Ser.: Mater. Sci. Eng.* 1091012067.
 56. **Fang, Y.; Li, P.; Zhou, H.; Zuo, W.** 2017. Thermoelastic damping in rectangular microplate resonators with three-dimensional heat conduction, *Int. J. Mech. Sci.* 133: 578–589.
 57. **Resmi, R.; Suresh Babu, V.; Baiju, M. R.** 2021. Analysis of thermoelastic damping limited quality factor and critical dimensions of circular plate resonators based on axisymmetric and non-axisymmetric vibrations, *AIP Advances* 11: 035108. <https://doi.org/10.1063/5.0033087>.
 58. **Zuo, W.; Li, P.; Zhang, J.; Fang, Y.** 2016. Analytical modeling of thermoelastic damping in bilayered microplate resonators, *Int. J. Mech. Sci.* 106: 128–137.
 59. **Zuo, W.; Li, P.; Zhang, J.; Fang, Y.** 2016. Analytical modeling of thermoelastic damping in bilayered microplate resonators, *International Journal of Mechanical Sciences* 106:128-137. <https://doi.org/10.1016/j.ijmecsci.2015.12.009>.
 60. **Liu, S.; Sun, Y.; Ma, J.; Yang, J.** 2018. Theoretical analysis of thermoelastic damping in bilayered circular plate resonators with two-dimensional heat conduction, *Int. J. Mech. Sci.* 135: 114–123.
 61. **Kim, J.; Reddy, J.** 2015. A general third-order theory of functionally graded plates with modified couple stress effect and the von Kármán nonlinearity: theory and finite element analysis, *Acta Mech.* 226(9): 2973.
 62. **Pei, Y. C.** 2012. Thermoelastic damping in rotating flexible micro-disk. *Int. J. Mech. Sci.* 61(1): 52–64.
 63. **Hossain, S. T.; McWilliam, S.; Popov, A. A.** 2016. An investigation on thermoelastic damping of high-Q ring resonators, *Int. J. Mech. Sci.* 106: 209–219.
 64. **Zener, C.** 1937. Internal friction in solids. I. Theory of internal friction in reeds, *Phys. Rev.* 52(3): 230–235.
 65. **Zener, C.** 1938. Internal friction in solids II. General theory of thermoelastic internal friction, *Phys. Rev.* 53(1): 90–99.
 66. **Zener, C.; Otis, W.; Nuckolls, R.** 1938. Internal friction in solids III. Experimental demonstration of thermoelastic internal friction, *Phys. Rev.* 53(1): 100–101.
 67. **Landau, L. D.; Lifshitz, E. M.** 1959. *Theory of Elasticity*. Pergamon Press, Oxford.
 68. **Roszhart, T. V.** 1990. The effect of thermoelastic internal friction on the Q of micromachined silicon resonators, *Solid-State Sensor and Actuator Workshop 4th Technical Digest, IEEE*, pp. 13–16. IEEE.
 69. **Yasumura, K.Y.; Stowe, T. D.; Kenny, T. W.; Rugar, D.** 1999. *Bull. Am. Phys. Soc.* 44 (1): 540.
 70. **Lifshitz, R.; Roukes, M. L.** 2000. Thermoelastic damping in micro- and nanomechanical systems, *Phys. Rev. B* 61(8): 5600.
 71. **Duwel, A.; Gorman, J.; Weinstein, M.; Borenstein, J.; Ward, P.** 2003. Experimental study of thermoelastic damping in MEMS gyros, *Sensors and Actuators A: Physical, Elsevier* 103(1-2): 70.
 72. **Nayfeh, A. H.; Younis, M. I.** 2004. Modeling and simulations of thermoelastic damping in microplates, *Journal of Micromechanics and Microengineering* 14(12): 1711-1717.
 73. **Vogl, G. W.; Nayfeh, A. H.** 2005. A reduced-order model for electrically actuated clamped circular plates, *J. Micromech. Microeng.* 15(4): 684–690.
 74. **Rao, S. S.** 2007. *Vibration of Continuous Systems*, John Wiley & Sons, Inc. Hoboken, New Jersey.
 75. **Zhili Hao.** 2008. Thermoelastic damping in the contour-mode vibrations of micro- and nano-electromechanical circular thin-plate resonators 313(1-2): 77–96. <https://doi.org/10.1016/j.jsv.2007.11.035>.
 76. **Zhang Da-Guang; You-He Zhou.** 2008. A theoretical analysis of FGM thin plates based on physical neutral surface, *Computational Materials Science* 44(2): 716-720.
 77. **Sun, Y.; Tohmyoh, H.** 2009. Thermoelastic damping of the axisymmetric vibration of circular plate resonators, *J. Sound Vibr.* 319: 392–405.
 78. **Yi, Y.** 2010. Finite element analysis of thermoelastic damping in contour-mode vibrations of micro- and nanoscale ring, disk, and elliptical plate resonators, *ASME J. Vib. Acoust.* 132(4): 041015.

- <https://doi.org/10.1115/1.4001506>.
79. **Sun, Y.; Saka, M.** 2010. Thermoelastic damping in micro-scale circular plate resonators, *J. Sound Vibr.* 329: 328–337.
 80. **Ale Ali, Nassim; Mohammadi, A.** 2012. Thermoelastic damping in clamped-clamped annular microplate, *Applied Mechanics and Materials* 110-116: 1870-1878.
<https://doi.org/10.4028/www.scientific.net/AMM.110-116.1870>
 81. **Li, Pu; Fang, Yuming; Hu, Rufu.** 2012. Thermoelastic damping in rectangular and circular microplate resonators, *Journal of Sound and Vibration* 331: 721–733.
 82. **Fang, Y. M.; Li, P.; Wang, Z.** 2013. Thermoelastic damping in the axisymmetric vibration of circular microplate resonators with two-dimensional heat conduction, *J. Therm. Stresses* 36: 830-850.
 83. **Li, Z.; Zhao, L.; Ye, Z.; Wang, H.; Zhao, Y.; Jiang, Z.** 2013. Resonant frequency analysis on an electrostatically actuated microplate under uniform hydrostatic pressure, *Journal of Physics D: Applied Physics* 46: 195108.
 84. **Sun, Y.; Yang, J.; Jiang, Y.** 2014. A theoretical analysis of thermoelastic damping model in laminated trilayered circular plate resonators, *World Journal of Mechanics* 4: 102-111.
<https://doi.org/10.4236/wjm.2014.44012>.
 85. **Maruszewski, B. T.; Drzewiecki, A.; Starosta, R.** 2014. Thermoelastic damping in auxetic plate, *J. Transactions of Nanjing University of Aeronautics & Astronautics* 31(2):133-136.
 86. **Reddy, J. N.** 2015. *An Introduction to Nonlinear Finite Element Analysis*, 2nd ed., Oxford University Press, Oxford, UK.
 87. **Jiang, P.** 2015. Mechanism and model of thermoelastic damping in micro-plate resonators with three-dimensional heat conduction, Southeast University, Nanjing, China.
 88. **Zuo, W.; Li, P.; Zhang, J.; Fang, Y.** 2016. Analytical modeling of thermoelastic damping in bilayered microplate resonators, *Int. J. Mech. Sci.* 106: 128–137.
 89. **Fang, Y.; Li, P.; Zhou, H.; Zuo, W.** 2017. Thermoelastic damping in rectangular microplate resonators with three-dimensional heat conduction, *Int. J. Mech. Sci.* 133: 578–589.
 90. **Ramu Inala; Sukesh C. Mohanty.** 2017. Free vibration analysis of rotating plates in high thermal environments using the finite element method, *International Journal of Acoustics and Vibration.* 22(1): 58.
 91. **Liu, S.; Sun, Y.; Ma, J.; Yang, J.** 2018. Theoretical analysis of thermoelastic damping in bilayered circular plate resonators with two-dimensional heat conduction, *Int. J. Mech. Sci.* 135: 114–123
 92. **Zhang, W.; Wu, Q.; Wensai, Ma.** 2018. Chaotic wave motions and chaotic dynamic responses of piezoelectric laminated composite rectangular thin plate under combined transverse and in-plane excitations, *International Journal of Applied Mechanics.*
<https://doi.org/10.1142/S1758825118501144>.
 93. **Liu, Shoubin; Ma, Jingxuan; Yang, Xianfeng; Sun, Yuxin; Yang, Jialing; Wang, Xin.** 2018. Theoretical 3D model of thermoelastic damping in laminated rectangular plate resonators, *International Journal of Structural Stability and Dynamics* 18(12): 18501584.
<https://doi.org/10.1142/S0219455418501584>.
 94. **Balakrishna Adhikari; Singh, B. N.** 2019. Dynamic response of functionally graded plates resting on two-parameter-based elastic foundation model using a quasi-3D theory, *Mechanics Based Design of Structures and Machines* 47(4): 399-429.
<https://doi.org/10.1080/15397734.2018.1555965>.
 95. **Sayyid, H.; Hashemi Kachapi.** 2020. Surface/interface approach in pull-in instability and nonlinear vibration analysis of fluid-conveying piezoelectric nanosensor, *Mechanics Based Design of Structures and Machines.*
<https://doi.org/10.1080/15397734.2020.1725566>.
 96. **Kumar Harendra; Santwana Mukhopadhyay.** 2020. Thermoelastic damping in micro and nano-mechanical resonators utilizing entropy generation approach and heat conduction model with a single delay term, *International Journal of Mechanical Sciences* 165: 105211.
 97. **Abhik Sur; Sudip Mondal; M. Kanoria.** 2021. Memory response on wave propagation in a thermoelastic plate due to moving band-type thermal loads and magnetic field, *Mechanics Based Design of Structures and Machines* 49(2): 172-193.
<https://doi.org/10.1080/15397734.2019.1672558>.
 98. **Karimi, M.; Rafieian, S.; Farajpour, M. R.; Miles, R. N.; Salehipour, H.; Jazar, R. N.; Khayyam, H.** 2021. Wave propagation and vibration in intelligent nanoplates: A mechanical modeling approach, *Mechanics Based Design of Structures and Machines.*
<https://doi.org/10.1080/15397734.2021.1890613>.
 99. **Safarpour, M.; Rahimi, A.; Alibeigloo, A.; Bisheh, H.; Forooghi, A.** 2021. Parametric study of three-dimensional bending and frequency of FG-GPLRC porous circular and annular plates on different boundary conditions, *Mechanics Based Design of Structures and Machines* 49(5):707-737.
<https://doi.org/10.1080/15397734.2019.1701491>.
 100. **Pawan Kumar; Harsha, S. P.** 2021. Vibration response analysis of sigmoidal functionally graded piezoelectric (FGP) porous plate under thermo-electric environment, *Mechanics Based Design of Structures and Machines.*
<https://doi.org/10.1080/15397734.2021.1971090>.
 101. **Chasiotis, I.; Knauss, W. G.** 2002. A new microtensile tester for the study of MEMS materials with the aid of atomic force microscopy, *Experimental Mechanics* 42: 51–57.
 102. **Gianola, D.; Sharpe, W.** 2004. Techniques for testing thin films in tension, *Experimental Techniques* 28: 23–27.
 103. **Mindlin, R. D.; Tiersten, H. F.** 1962. Effects of couple-stresses in linear elasticity. *Archive for Rational Mechanics and Analysis* 11(1):415-448.
<https://doi.org/10.1007/bf00253946>.
 104. **Toupin, R. A.** 1964. Theories of elasticity with couple-stress, *Archive for Rational Mechanics and Analysis* 17(2): 85–112.
<https://doi.org/10.1007/BF00253050>.
 105. **Koiter, W. T.** 1964. Couple-stresses in the theory of elasticity: I and II. *Proc. K. Ned. Akad. Wet. B* 67: 17-47.
 106. **Faraji-Oskouie, M.; Norouzzadeh, A.; Ansari, R.; et al.** 2019. Bending of small-scale Timoshenko beams

- based on the integral/differential nonlocal-micropolar elasticity theory: a finite element approach, *Appl. Math. Mech.-Engl. Ed.* 40: 767–782.
<https://doi.org/10.1007/s10483-019-2491-9>.
107. **Ansari, R.; Pourashraf, T.; Gholami, R.; et al.** 2016. Analytical solution approach for nonlinear buckling and postbuckling analysis of cylindrical nanoshells based on surface elasticity theory, *Appl. Math. Mech.-Engl. Ed.* 37: 903–918.
<https://doi.org/10.1007/s10483-016-2100-9>.
 108. **Rahaeifard, M.; Kahrobaiyan, M.; Asghari, M.; Ahmadian, M.** 2011. Static pull-in analysis of micro-cantilevers based on the modified couple stress theory, *Sens. Actuat. A* 171(2): 370–374.
 109. **Bostani, M.; Karami Mohammadi, A.** 2018. Thermoelastic damping in microbeam resonators based on modified strain gradient elasticity and generalized thermoelasticity theories, *Acta Mech.* 229: 173–192.
 110. **Borjalilou, V.; Asghari, M.; Taati, E.** 2020. Thermoelastic damping in nonlocal nanobeams considering dual-phase-lagging effect, *J. Vib. Control.*
<https://doi.org/10.1177/1077546319891334>.
 111. **Babak Alizadeh Hamidi; Farshad Khosravi; Seyed Amirhossein Hosseini; Reza Hassannejad.** 2020. Closed form solution for dynamic analysis of rectangular nanorod based on nonlocal strain gradient, *Waves in Random and Complex Media.*
<https://doi.org/10.1080/17455030.2020.1843737>.
 112. **Yang, F.; Chong, A. C. M.; Lam, D. C. C.; Tong, P.** Couple stress based strain gradient theory for elasticity, *International Journal of Solids and Structures* 39(10): 2731–2743.
[https://doi.org/10.1016/S0020-7683\(02\)00152-X](https://doi.org/10.1016/S0020-7683(02)00152-X).
 113. **Lam, D. C. C.; Yang, F.; Chong, A. C. M.; Wang, J.; Tong, P.** 2003. Experiments and theory in strain gradient elasticity, *J. Mech. Phys. Solids* 51(8): 1477–1508.
 114. **Lim, C.W.; He, L.H.** 2004. Size-dependent nonlinear response of thin elastic films with nano-scale thickness, *International Journal of Mechanical Sciences* 46(11): 1715–1726.
<https://doi.org/10.1016/j.ijmecsci.2004.09.003>.
 115. **Zhang, X.; Sharma, P.** 2005. Inclusions and inhomogeneities in strain gradient elasticity with couple stresses and related problems, 42(13): 3833–3851.
<https://doi.org/10.1016/j.ijsolstr.2004.12.005>.
 116. **Lu, P.; He, L. H.; Lee, H. P.; Lu, C.** 2006. Thin plate theory including surface effects, *International Journal of Solids and Structures* 43(16): 4631–4647.
<https://doi.org/10.1016/j.ijsolstr.2005.07.036>.
 117. **Ieşan, D.** 2007. Thermoelasticity of bodies with microstructure and microtemperatures, *International Journal of Solids and Structures* 44(25): 8648–8662.
<https://doi.org/10.1016/j.ijsolstr.2007.06.027>.
 118. **Batra, R. C.; Porfiri, M.; Spinello, D.** 2008. Vibrations and pull-in instabilities of microelectromechanical von Kármán elliptic plates incorporating the Casimir force, *Journal of Sound and Vibration* 315(4-5): 939–960.
<https://doi.org/10.1016/j.jsv.2008.02.008>.
 119. **Lazopoulos, K. A.** 2009. On bending of strain gradient elastic micro-plates, *Mech. Res. Commun.* 36(7): 777–783.
 120. **Yin, L.; Qian, Q.; Wang, L.; Xia, W.** 2010. Vibration analysis of microscale plates based on modified couple stress theory, *ActaMech. SolidaSinica* 23(5): 386–393.
 121. **Jomehzadeh, E.; Noori, H. R.; Saidi, A. R.** 2011. The size-dependent vibration analysis of micro-plates based on a modified couple stress theory 43(4): 877–883.
<https://doi.org/10.1016/j.physe.2010.11.005>.
 122. **Ke, L. L.; Wang, Y. S.; Yang, J.; Kitipornchai, S.** 2012. Free vibration of size-dependent Mindlinmicro-plates based on the modified couple stress theory *J. Sound Vibrat.* 331(1): 94–106.
 123. **Huu-Tai Thai; Dong-Ho Choi.** 2013. Size-dependent functionally graded Kirchhoff and Mindlin plate models based on a modified couple stress theory, 95(none).
<https://doi.org/10.1016/j.compstruct.2012.08.02>.
 124. **Gheshlaghi, Behnam; Hasheminejad, Seyyed.** 2013. Size dependent damping in axisymmetric vibrations of circular nanoplates, *Thin Solid Films* 537: 212–216.
<https://doi.org/10.1016/j.tsf.2013.04.014>.
 125. **Asghari, M.; Taati, E.** 2013. A size-dependent model for functionally graded microplates for mechanical analyses, *J. Vib. Control* 19(11): 1614–1632.
 126. **Shaat, M.; Mahmoud, F. F.; Gao, X. L.; Faheem, A. F.** 2014. Size-dependent bending analysis of Kirchhoff nano-plates based on a modified couple-stress theory including surface effects, *International Journal of Mechanical Sciences* 79: 31–37.
<https://doi.org/10.1016/j.ijmecsci.2013.11.022>.
 127. **Guo, F.; Song, J.; Wang, G.; Zhou, Y.** 2014. Analysis of thermoelastic dissipation in circular micro-plate resonators using the generalized thermoelasticity theory of dual-phase-lagging model, *J. Sound Vib.* 333(11): 2465–2474.
 128. **Tsiatas, George; Yiotis, Aristophanes.** 2014. Size effect on the static, dynamic and buckling analysis of orthotropic Kirchhoff-type skew micro-plates based on a modified couple stress theory: Comparison with the nonlocal elasticity theory, *Acta Mechanica* 226.
<https://doi.org/10.1007/s00707-014-1249-3>.
 129. **Ansari, R.; Faghieh Shojaei, M.; Mohammadi, V.; Gholami, R.; Darabi, M.A.** 2014. Nonlinear vibrations of functionally graded Mindlin microplates based on the modified couple stress theory, *Composite Structures* 114: 124–134.
<https://doi.org/10.1016/j.compstruct.2014.04.013>.
 130. **Farokhi, Hamed; Ghayesh, Mergen H.** 2015. Non-linear dynamical behaviour of geometrically imperfect microplates based on modified couple stress theory, *International Journal of Mechanical Sciences* 90: 133–144.
<https://doi.org/10.1016/j.ijmecsci.2014.11.002>.
 131. **Askari, A. R.; Masoud Tahani.** 2015. Analytical determination of size-dependent natural frequencies of fully clamped rectangular microplates based on the modified couple stress theory, *Journal of Mechanical Science and Technology* 29(5): 2135–2145.
 132. **Şimşek, M.; Aydın, M.; Yurtcu, H. H.; et al.** 2015. Size-dependent vibration of a microplate under the action of a moving load based on the modified couple stress theory, *Acta Mech.* 226:3807–3822.
<https://doi.org/10.1007/s00707-015-1437-9>.
 133. **Eshraghi, Iman; Dag, Serkan; Soltani, Nasser.** 2015. Consideration of spatial variation of the length

- scale parameter in static and dynamic analyses of functionally graded annular and circular micro-plates, *Composites Part B: Engineering* 78: 338–348. <https://doi.org/10.1016/j.compositesb.2015.03.095>.
134. **Taati, E.** 2015. Analytical solutions for the size dependent buckling and postbuckling behavior of functionally graded micro-plates, *International Journal of Engineering Science* 100: 45–60. <https://doi.org/10.1016/j.ijengsci.2015.11.007>.
 135. **Lou, Jia; He, Liwen; Du, Jianke.** 2015. A unified higher order plate theory for functionally graded microplates based on the modified couple stress theory. *Composite Structures* S0263822315006868. <https://doi.org/10.1016/j.compstruct.2015.08.009>.
 136. **Reddy, J. N.; Romanoff, J.; Loya, J. A.** 2016. Non-linear finite element analysis of functionally graded circular plates with modified couple stress theory, *Eur. J. Mech. A/Solids* 56: 92–104. <https://doi.org/10.1016/j.euromechsol.2015.11.001>.
 137. **Razavilar, R.; Alashti, R.A.; Fathi, A.** 2016. Investigation of thermoelastic damping in rectangular microplate resonator using modified couple stress theory, *Int. J. Mech. Mater. Des.* 12(1): 39–51.
 138. **Ansari, R.; Gholami, R.; Shahabodini, A.** 2016. Size-Dependent Geometrically Nonlinear Forced Vibration Analysis of Functionally Graded First-Order Shear Deformable Microplates, *Journal of Mechanics* 32(5): 539-554. <https://doi.org/10.1017/jmech.2016.10>.
 139. **Askari, A. R.; Tahani, Masoud.** 2016. Size-dependent dynamic pull-in analysis of geometric non-linear micro-plates based on the modified couple stress theory, *Physica E: Low-dimensional Systems and Nanostructures* S1386947716302636. <https://doi.org/10.1016/j.physe.2016.10.035>.
 140. **Nguyen Hoang X.; Nguyen, Tuan N.; Abdel-Wahab M.; Bordas, S. P. A.; Nguyen-Xuan, H.; Vo, T. P.** 2016. A refined quasi-3D isogeometric analysis for functionally graded microplates based on the modified couple stress theory. *Computer Methods in Applied Mechanics and Engineering* S0045782516308167. <https://doi.org/10.1016/j.cma.2016.10.002>.
 141. **Thai Huu-Tai; Vo Thuc P.; Patel Vipulkumar Ishvarbhai.** 2017. Size-dependant behaviour of functionally graded microplates based on the modified strain gradient elasticity theory and isogeometric analysis, *Computers & Structures* 190: 219–241. <https://doi.org/10.1016/j.compstruc.2017.05.014>.
 142. **Liu Shuo; Yu Tiantang; Bui Tinh Quoc.** 2017. Size effects of functionally graded moderately thick microplates: A novel non-classical simple-FSDT isogeometric analysis, *European Journal of Mechanics - A/Solids* S0997753817302425. <https://doi.org/10.1016/j.euromechsol.2017.08.008>.
 143. **Malikan Mohammad.** 2017. Electro-mechanical shear buckling of piezoelectric nanoplate using modified couple stress theory based on simplified first order shear deformation theory, *Applied Mathematical Modelling* 48: 196–207. <https://doi.org/10.1016/j.apm.2017.03.065>.
 144. **Vahid Borjalilou, Mohsen Asghari.** 2018. Small-scale analysis of plates with thermoelastic damping based on the modified couple stress theory and the dual-phase-lag heat conduction model, Springer-Verlag GmbH Austria, part of Springer Nature. <https://doi.org/10.1007/s00707-018-2197-0>.
 145. **Thai, C. H.; Ferreira, A. J. M.; Lee, J.; Nguyen-Xuan, H.** 2018. An efficient size-dependent computational approach for functionally graded isotropic and sandwich microplates based on modified couple stress theory and moving Kriging-based meshfree method. *International Journal of Mechanical Sciences* S0020740317332010. <https://doi.org/10.1016/j.ijmecsci.2018.04.040>.
 146. **Ajri, M.; Seyyed Fakhrahadi, M.** 2018. Nonlinear free vibration of viscoelastic nanoplates based on modified couple stress theory, *Journal of Computational Applied Mechanics* 49(1): 44-53. <https://doi.org/10.22059/jcamech.2018.228477.129>.
 147. **Kim Jinseok; Żur Krzysztof Kamil; Reddy, J. N.** 2018. Bending, free vibration, and buckling of modified couples stress-based functionally graded porous micro-plates, *Composite Structures* S0263822318335517. <https://doi.org/10.1016/j.compstruct.2018.11.02>.
 148. **Devi, S.; Kumar, R.** 2018. Damping and frequency shift in microscale modified couple stress thermoelastic plate resonators, *Journal of Solid Mechanics* 10(3): 621-636.
 149. **Farzam, A.; Hassani Behrooz.** 2019. Isogeometric analysis of in-plane functionally graded porous microplates using modified couple stress theory, *Aerospace Science and Technology* S1270963819307989. <https://doi.org/10.1016/j.ast.2019.05.012>.
 150. **Liu, Y.; Wang, Y.** 2019. Size-dependent free vibration and buckling of three-dimensional graphene foam microshells based on modified couple stress theory, *Materials* 12(5): 729. <https://doi.org/10.3390/ma12050729>.
 151. **Resmi, R.; Baiju, M. R.; Suresh Babu, V.** 2019. Thermoelastic damping dependent quality factor analysis of rectangular plates applying modified couple stress theory, *AIP Conference Proceedings* 2166: 020029. <https://doi.org/10.1063/1.5131616>.
 152. **Borjalilou, V.; Asghari, M.** 2020. Thermoelastic damping in strain gradient microplates according to a generalized theory of thermoelasticity, *Journal of Thermal Stresses* 43: 1-20. <https://doi.org/10.1080/01495739.2020.1722771>.
 153. **Kumar R.; Tiwari, R.; Kumar, R.** 2020. Significance of memory-dependent derivative approach for the analysis of thermoelastic damping in micromechanical resonators, *Mech Time-Depend Mater.* <https://doi.org/10.1007/s11043-020-09477-7>.
 154. **Devi, S.; Kumar, R.** 2020. Thermoelastic damping and frequency shift in kirchhoff plate resonators based on modified couple stress theory with dual-phase-lag model, *Journal of Solid Mechanics* 12(3): 700-712. <https://doi.org/10.22034/jsm.2020.1896290.1569>.
 155. **Yekani, S. M. A.; Fallah, F.** 2020. A Levy solution for bending, buckling, and vibration of Mindlin micro plates with a modified couple stress theory, *SN Appl. Sci.* 2:2169. <https://doi.org/10.1007/s42452-020-03939-w>.
 156. **Zhaohai Yang; Dan Cheng; Guangyu Cong; DaweiJin; Vahid Borjalilou.** 2021. Dual-phase-lag

- thermoelastic damping in nonlocal rectangular nanoplates, *Waves in Random and Complex Media*.
<https://doi.org/10.1080/17455030.2021.1903117>.
157. **Zhou, H.; Li, P.** 2021. Nonlocal dual-phase-lagging thermoelastic damping in rectangular and circular micro/nanoplate resonators, *Applied Mathematical Modelling* 95: 667–687.
<https://doi.org/10.1016/j.apm.2021.02.035>.
158. **Resmi, R.; Suresh Babu V.; Baiju, M. R.** 2021. Impact of dimensionless length scale parameter on material dependent thermoelastic attenuation and study of frequency shifts of rectangular microplate resonators. *IOP Conference Series: Materials Science and Engineering* 1091: 012067.
<https://doi.org/10.1088/1757-899X/1091/1/012067>.
159. **Xiao Ge; Pu Li; Yuming Fang; Longfei Yang.** 2021. Thermoelastic damping in rectangular microplate/nanoplate resonators based on modified nonlocal strain gradient theory and nonlocal heat conductive law, *Journal of Thermal Stresses* 44(6): 690-714.
<https://doi.org/10.1080/01495739.2021.1906807>.
160. **Yuan Yuan; Kuo Xu.** 2021. Post buckling analysis of axially loaded nanoscaled shells embedded in elastic foundations based on Ru's surface elasticity theory, *Mechanics Based Design of Structures and Machines* 49(1): 20-40.
<https://doi.org/10.1080/15397734.2019.1665543>.
161. **Caiyuan Xiao; Guiju Zhang; Peisi Hu; Yudong Yu; Youyu Mo; Vahid Borjalilou.** 2021. Size-dependent generalized thermoelasticity model for thermoelastic damping in circular nanoplates, *Waves in Random and ComplexMedia*.
<https://doi.org/10.1080/17455030.2021.1968538/>.

R. Resmi, V.Suresh Babu, M. R. Baiju

IMPACTS OF MATERIAL PERFORMANCE INDICES AND LENGTH SCALE PARAMETER ON THERMOELASTIC DAMPING IN MICRO/NANOPLATES APPLYING MODIFIED COUPLE STRESS THEORY

S u m m a r y

Energy dissipation in micro- and nanoscale resonators can be optimized by improving the thermoelastic-damping-limited quality factor. Maximizing energy dissipation is interrelated with the critical length of the resonator plates; by optimizing the dimensions, the peaking of energy dissipation can be diminished. However, classical continuum theories cannot explain the size effects related to mechanical behavior at micron or submicron sizes. In this study, isotropic rectangular micro-plates are used to analyze the size-dependent thermoelastic damping and its impact on the quality factor and critical dimensions such as critical length of micro/nano plates. Micro- and nanoplates using five different structural materials are analyzed to optimize quality factor, which depends on two material performance indices: thermoelastic damping index and thermal diffusion length. In our study, an expression for the thermoelastic damping limited quality factor is derived in terms of the material performance indices and simulated numerically using MATLAB R2015a. Accordingly, the maximum thermoelastic damping limited quality factor is attained for polySi with the lowest thermoelastic damping index and maximum critical length is obtained for SiC with the lowest thermal diffusion length. The impact of material length-scale parameters l , material performance indices, vibration modes, and boundary conditions on quality factor limited by thermoelastic damping and critical length are also investigated. Quality factor is maximized by selecting polySi as the structural material with higher internal length-scale parameters l . These results can help designers to engineer high-performance, low-loss resonators at micro/nanoscales.

Keywords: micro/nano rectangular plates, thermoelastic damping limited quality factor, critical length, material length scale parameter, material performance indices, clamped-clamped and simply supported boundary conditions.

Received January 08, 2021

Accepted June 14, 2022



This article is an Open Access article distributed under the terms and conditions of the Creative Commons Attribution 4.0 (CC BY 4.0) License (<http://creativecommons.org/licenses/by/4.0/>).